

# Floquet-ADAPT-VQE: A Quantum Algorithm to Simulate Non-Equilibrium Physics in Periodically Driven Systems

Abhishek Kumar<sup>1,2</sup>, Karunya Shirali<sup>1,2</sup>, Nicholas J. Mayhall<sup>3,2</sup>, Sophia E. Economou<sup>1,2</sup> and Edwin Barnes<sup>1,2</sup>

<sup>1</sup>*Department of Physics, Virginia Tech, Blacksburg, VA 24061, USA*

<sup>2</sup>*Virginia Tech Center for Quantum Information Science and Engineering, Blacksburg, VA 24061, USA*

<sup>3</sup>*Department of Chemistry, Virginia Tech, Blacksburg, VA 24061, USA*

(Dated: June 12, 2025)

Periodically driven quantum systems exhibit many fascinating phenomena absent in equilibrium systems, but their simulation is more challenging than that of static systems. Consequently, quantum simulation of these systems offers greater opportunity for achieving quantum advantage. To build the foundation for simulating time-periodic Hamiltonians, we utilize the Floquet-Hilbert space formalism to transform the Hamiltonian into a time-independent form and provide its Pauli decomposition. We propose a hybrid quantum-classical algorithm, Floquet-ADAPT-VQE, to simulate the non-equilibrium physics of periodically driven quantum systems. We define a cost function based on the square of the shifted extended Floquet Hamiltonian and show how to prepare Floquet states using Floquet-ADAPT-VQE. We also obtain a suitable auxiliary initial state whose squared Floquet energy is independent of the number of auxiliary qubits as well as the driving frequency, which leads to better convergence with fewer ADAPT iterations. Additionally, we provide a framework to calculate the time-dependent expectation value of observables in the Floquet state with fixed-depth quantum circuit. We demonstrate our algorithm by performing numerical simulations on a periodically driven XYZ model with a magnetic field. We also explore potential applications of our algorithm for studying various non-equilibrium phenomena in periodically driven systems.

## I. INTRODUCTION

Non-equilibrium many-body quantum systems, particularly periodically driven systems, exhibit a wide array of fascinating phenomena that do not occur in equilibrium systems. These phenomena include, but are not limited to, non-equilibrium phases such as time crystals [1–8] and Floquet topology [9–13], both of which lack counterparts in equilibrium systems. In general, Floquet states, which are eigensolutions of Schrödinger’s equation (up to a phase) for periodically driven Hamiltonians, play a crucial role in the manifestation of these remarkable phenomena. For instance, in time crystals that exhibit period doubling, product states can be expressed as linear combinations of two Floquet states separated by half of the driving frequency in the quasienergy spectrum. Therefore, the system manifests a spontaneous breaking of discrete time translation symmetry when it is initialized in a product state. Additionally, Floquet states can exhibit non-equilibrium topology due to the presence of additional gaps between Floquet zone bands. Broadly speaking, periodic drives offer a means to control the electronic properties of quantum matter [14] and could potentially be utilized to create sensors to detect exotic features of a system [15]. As a result of these rich phenomena, and many others yet to be fully explored, the study of periodically driven systems has garnered significant attention in recent years, emerging as a major focus for researchers in condensed matter physics, atomic, molecular, and optical physics, as well as quantum computation.

Simulating many-body quantum systems, even in equilibrium, poses significant challenges; the task becomes even more daunting in the case of non-equilibrium, driven, physical systems. The complexity of simulating non-equilibrium physics in periodically driven many-body quantum systems stems from two primary challenges: the exponential growth of the Hilbert space with the system size and the errors introduced by approximating the time evolution operator (e.g., Trotterization). On the other hand, using devices based on quantum mechanics to simulate many-body quantum systems, as suggested by Feynman [16], has emerged as a promising avenue to study non-equilibrium behavior. Quantum simulators or analog quantum computers have already demonstrated the ability to simulate many-body physics that are intractable on classical computers [17–19]. However, these simulators are not universal; they function by mimicking many-body interactions and can only simulate a limited range of many-body systems of interest.

In contrast, digital quantum computers are universal and have the potential to efficiently simulate any many-body system. While a fully fault-tolerant quantum computer would be an ideal platform to perform these simulations [20], error correction schemes have not yet been able to reach the stage at which such fault-tolerant quantum computers can be realized. However, currently available Noisy Intermediate-Scale Quantum (NISQ) devices could still be a valuable resource in addressing this challenge [21]. In this context, hybrid quantum-classical algorithms like the Variational Quantum Eigensolver (VQE) [22, 23] are especially promising. In particular, the Adaptive Derivative-Assembled Problem Tailored Variational Quantum Eigensolver (ADAPT-VQE) [24–26], holds great promise, as it can generate

shallow quantum circuits suited for noisy qubits with limited coherence times. It has also been found to be robust against some optimization problems that plague VQEs [27].

Recently, Fauseweh et al. proposed two hybrid algorithms [28], in the time and frequency domains, to calculate the quasienergies in periodically driven systems using the variational Hamiltonian ansatz [29]. Although this work successfully demonstrated the calculation of quasienergies, both methods have limitations. The time-domain algorithm requires Trotterization for one time period and iterative quantum phase estimation (IQPE) [30], in addition to the usual VQE implementation. This can lead to much deeper circuits and is only effective for short time periods (high frequencies). The frequency-domain algorithm also has some limitations: it uses an auxiliary space with a limited dimension (at most five), and it does not provide any general prescription to obtain the Pauli decomposition of the auxiliary matrices for arbitrary qubit truncation. Consequently, the algorithm can simulate the periodic system accurately only at high driving frequencies. Additionally, a potentially major challenge is ansatz initialization, which can be critical for convergence, since simulations using the variational Hamiltonian ansatz typically require running the optimization multiple times with different randomly chosen initial parameter values and post-selection. Finally, the method does not provide a framework to study the expectation values of operators with respect to Floquet states, which play a crucial role in studying various non-equilibrium phenomena.

In this paper, we build a general framework to simulate periodically driven systems in a manner similar to that used for time-independent systems. We make use of a Floquet-Hilbert space formalism to convert the Hamiltonian to a time-independent form, and provide a method to decompose the auxiliary matrices, and hence the extended Floquet Hamiltonian, into a Pauli basis that can be natively implemented to a qubit-based quantum processor. In particular, we develop a hybrid quantum-classical algorithm that we call Floquet-ADAPT-VQE to simulate the non-equilibrium physics of a periodically driven system on a quantum computer. We define a cost function in terms of the square of the shifted extended Floquet Hamiltonian. Floquet-ADAPT-VQE utilizes these ingredients to prepare the extended Floquet state on a quantum computer and to obtain its quasienergy. Choosing a suitable initial state for the auxiliary register is important to the efficacy of the algorithm due to the dependence of the squared Floquet energy on the number of auxiliary qubits and the driving frequency. We propose choosing this state to be an eigenstate of a diagonal auxiliary matrix with vanishing eigenvalue and prove that, in this case, the squared Floquet energy is independent of both the number of auxiliary qubits and the driving frequency. Additionally, we present an algorithm to calculate the entire quasienergy spectrum within a Floquet zone. Furthermore, we present a method to calculate the time-dependent expectation value of an operator with respect to the prepared Floquet state with a fixed-depth quantum circuit.

To illustrate the effectiveness of our algorithm, we classically simulate it for a periodically driven XYZ model with an applied magnetic field. We show that the reference value of the cost function (the squared Floquet energy) of our proposed initial state, unlike that of a random initial state, does not increase even when the number of auxiliary qubits and driving frequency are increased. We demonstrate the effectiveness of our algorithm by testing it across a range of drive parameters. Additionally, we compute the full quasienergy spectrum within the central Floquet zone by tuning a shift parameter in the cost function. Finally, we calculate the expectation values of the net magnetization ( $\sum_j Z_j$ ) and the two-point correlation function  $\sum_j Z_j Z_{j+1}$  using our algorithm.

The paper is organized as follows. In Sec. II, we discuss Floquet theory, its representation in the Floquet-Hilbert space, and its usefulness for NISQ devices. We also provide a brief discussion of ADAPT-VQE. In Sec. III, we show how to construct auxiliary matrices and extended Floquet Hamiltonians in terms of Pauli strings. We also define the cost function based on the squared Floquet Hamiltonian and discuss choices of initial states and operator pools. In addition, we propose a framework to calculate the expectation values of operators with respect to Floquet states on a quantum computer. In Sec. IV, we present classical simulations of our algorithms applied to a periodically driven XYZ model with an external magnetic field. In Sec. V, we discuss several applications of our algorithm for light-matter interactions in many-body interacting systems, as well as the potential for detecting time crystals using our framework. Some additional details are given in the appendices.

In this work, we denote an operator in physical space as  $\hat{O}$ , in auxiliary space as  $O$ , and in the Floquet-Hilbert space as  $\hat{\hat{O}}$ . Similarly, a state in physical and auxiliary space is represented as  $|\psi\rangle$ , and in Floquet-Hilbert space as  $|\hat{\psi}\rangle$ . Throughout this work, we denote an operator and its matrix representation using the same notation. Also,  $T$  in  $(\dots)^T$  represents the transpose of a matrix throughout this paper. Additionally, we use three kinds of bases for  $2^N$  dimensional Hilbert space: the Fourier basis  $\{|n\rangle\}_{n=-2^{N-1}+1}^{2^{N-1}}$ , the standard vector basis in  $\mathbb{R}^{2^N}$ , and the computational basis  $|\gamma_1 \dots \gamma_N\rangle$  where  $\gamma_j \in \{\uparrow, \downarrow\}$ .

## II. PRIMER ON FLOQUET SYSTEMS AND ADAPT-VQE

### A. Floquet System

Floquet systems are governed by a time-periodic Hamiltonian  $\hat{H}(t) = \hat{H}(t + T)$ , where  $T = 2\pi/\Omega$  and  $\Omega$  is the fundamental frequency of the drive. According to the Floquet theorem [31], the solutions of the time-dependent Schrödinger equation,  $i\partial_t |\psi(t)\rangle = \hat{H}(t) |\psi(t)\rangle$  (assuming  $\hbar = 1$ ), take the form  $|\psi_\alpha(t)\rangle = e^{-i\epsilon_\alpha t} |\phi_\alpha(t)\rangle$ . The time-periodic component of the solution,  $|\phi_\alpha(t)\rangle = |\phi_\alpha(t + T)\rangle$ , is known as a Floquet state and satisfies the Floquet-Schrödinger equation:

$$[\hat{H}(t) - i\partial_t] |\phi_\alpha(t)\rangle = \epsilon_\alpha |\phi_\alpha(t)\rangle. \quad (1)$$

Here, the subscript  $\alpha \in \{1, 2, \dots, D\}$  distinguishes different Floquet eigenstates, where  $D$  is the dimension of the Hilbert space. The quasienergies are defined modulo  $\Omega$  as  $\epsilon_\alpha \in (-\Omega/2, \Omega/2]$  and are conserved quantities.

The time evolution operator in Floquet systems can be decomposed into two parts as [32, 33]

$$\hat{U}(t, 0) = \hat{\Phi}(t) e^{-it\hat{H}_F}, \quad (2)$$

where  $\hat{\Phi}(t) = \hat{\Phi}(t + T)$  is the time-periodic “micromotion” operator, and  $\hat{H}_F$  is the Floquet Hamiltonian. Notably,  $\hat{\Phi}(0) = \hat{I}$  and  $\hat{U}(nT) = e^{inT\hat{H}_F}$ . The micromotion operator provides the time evolution within a period, while the Floquet unitary operator  $\hat{U}(T)$  governs the evolution at integer multiples of the period. Using  $\hat{U}_F = \hat{U}(T) = e^{-iT\hat{H}_F}$ , or the Floquet Hamiltonian  $\hat{H}_F = (i/T) \log(\hat{U}_F)$ , we can calculate the quasienergies and Floquet states for stroboscopic dynamics.

The periodic nature of the drive motivates calculating the Floquet state and its quasienergies in the frequency domain [32, 33]. The Fourier expansion of the time-periodic Hamiltonian can be written as  $\hat{H}(t) = \sum_{n \in \mathbb{Z}} e^{in\Omega t} \hat{H}^{(n)}$ , while the Floquet state can be expanded as  $|\phi_\alpha(t)\rangle = \sum_{m \in \mathbb{Z}} e^{im\Omega t} |\phi_\alpha^{(m)}\rangle$ . The Floquet-Schrödinger equation, Eq. (1), may thus be expressed as a series of equations for the various Fourier modes (labeled by  $n$ ) of a Floquet eigenstate (labeled by  $\alpha$ ):

$$\sum_{m \in \mathbb{Z}} [\hat{H}^{(n-m)} + n\Omega \delta_{nm}] |\phi_\alpha^{(m)}\rangle = \epsilon_\alpha |\phi_\alpha^{(n)}\rangle. \quad (3)$$

The above equations are a system of coupled linear equations that can also be represented in matrix form as

$$\begin{pmatrix} \dots & \dots & \dots & \dots & \dots & \dots & \dots \\ \dots & \hat{H}^{(0)} - 2\Omega & \hat{H}^{(-1)} & \hat{H}^{(-2)} & \dots & \dots & \dots \\ \dots & \hat{H}^{(1)} & \hat{H}^{(0)} - \Omega & \hat{H}^{(-1)} & \hat{H}^{(-2)} & \dots & \dots \\ \dots & \hat{H}^{(2)} & \hat{H}^{(1)} & \hat{H}^{(0)} & \hat{H}^{(-1)} & \hat{H}^{(-2)} & \dots \\ \dots & \dots & \hat{H}^{(2)} & \hat{H}^{(1)} & \hat{H}^{(0)} + \Omega & \hat{H}^{(-1)} & \dots \\ \dots & \dots & \dots & \hat{H}^{(2)} & \hat{H}^{(1)} & \hat{H}^{(0)} + 2\Omega & \dots \\ \dots & \dots & \dots & \dots & \dots & \dots & \ddots \end{pmatrix} \begin{pmatrix} \vdots \\ |\phi_\alpha^{(-2)}\rangle \\ |\phi_\alpha^{(-1)}\rangle \\ |\phi_\alpha^{(0)}\rangle \\ |\phi_\alpha^{(1)}\rangle \\ |\phi_\alpha^{(2)}\rangle \\ \vdots \end{pmatrix} = \epsilon_\alpha \begin{pmatrix} \vdots \\ |\phi_\alpha^{(-2)}\rangle \\ |\phi_\alpha^{(-1)}\rangle \\ |\phi_\alpha^{(0)}\rangle \\ |\phi_\alpha^{(1)}\rangle \\ |\phi_\alpha^{(2)}\rangle \\ \vdots \end{pmatrix}. \quad (4)$$

Thus, the effective time-independent extended Floquet Hamiltonian is an infinite-dimensional matrix. It is worth emphasizing that the elements of the extended Floquet Hamiltonian are Fourier modes of the time-periodic Hamiltonian and the elements of the extended Floquet state (column vector) are Fourier modes of the Floquet state  $|\phi_\alpha(t)\rangle$ .

Upon solving Eq. (4), we obtain the quasienergies  $\{\epsilon_\alpha \pm n\Omega\}_{n=0}^\infty$  and associated Floquet eigenstates. We note that the quasienergies are unbounded in the frequency domain, and the different values of  $n$  correspond to different Floquet zones. The zone with  $n = 0$  is termed the *central Floquet zone*, and the quasienergies of this zone are identical to the quasienergies calculated directly using  $\hat{U}(T)$  or  $\hat{H}_F$ .

In practice, we truncate the extended Floquet Hamiltonian, retaining a finite number of Floquet zones (or Fourier indices of a Floquet state) from  $-N_c$  to  $N_c$ . An equal number of positive ( $N_c \geq n > 0$ ) and negative ( $-N_c \leq n < 0$ ) Floquet zones are necessary to ensure that a general  $\hat{H}(t)$  is Hermitian even after truncation. Additionally, asymmetric truncation (i.e., including an unequal number of positive and negative Floquet zones) introduces more error compared to symmetric truncation. Qualitatively, it is known that the physics at higher frequencies and lower driving amplitudes can be reliably captured using fewer Floquet zones, and vice versa. We will discuss more about truncation in Sec. III A.

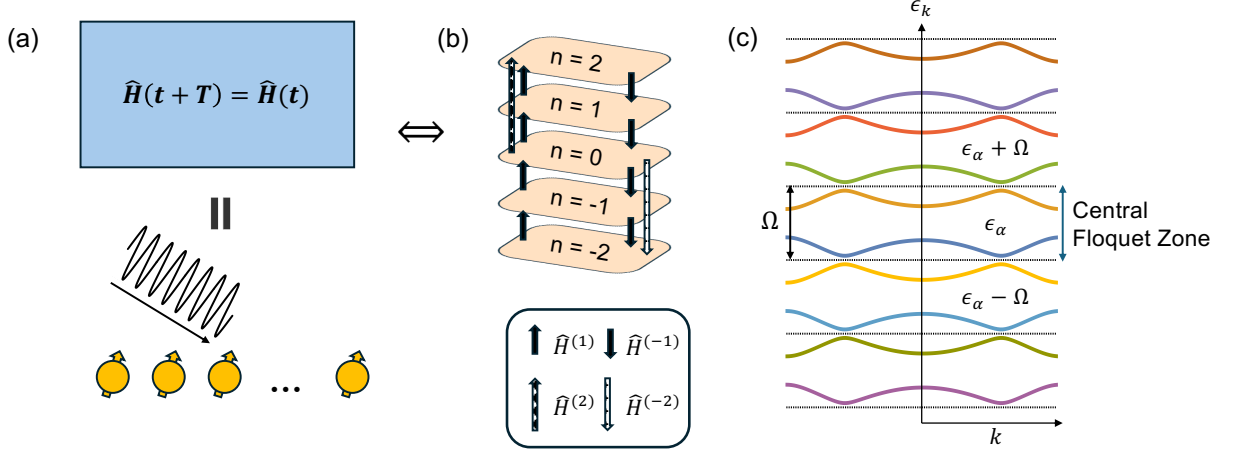


FIG. 1. Schematic diagrams for a Floquet system: (a) A periodically driven system with a time-periodic Hamiltonian  $\hat{H}(t+T) = \hat{H}(t)$ ; (b) representation of the Fourier modes of the Floquet state (indicated by planes) with indices  $n \in \mathbb{Z}$  in the frequency domain, where the Hamiltonian's Fourier components  $\hat{H}^{(n)}$  connect different Fourier planes; and (c) quasienergies across various Floquet zones for a driven two-band model (one qubit with coefficients dependent on parameter  $k$ ).

For a  $D \times D$ -dimensional  $\hat{H}(t)$ , and a cut-off at the  $\pm N_c$ -th Fourier index, we obtain an extended Floquet Hamiltonian of dimensions  $D(2N_c + 1) \times D(2N_c + 1)$ .

We can formalize the structure of the extended Floquet Hamiltonian and its corresponding Hilbert space (for more details, see Refs. [33, 34]). We consider a physical Hilbert space ( $\mathcal{H}$ ) and an auxiliary Hilbert space ( $\mathcal{A}$ ) that represents the Fourier indices (Floquet zones), such that the tensor product of the two forms a Floquet-Hilbert space  $\mathcal{F} = \mathcal{A} \otimes \mathcal{H}$ . The Schrödinger equation in the Floquet-Hilbert space can be written as

$$\hat{H}_F |\phi_{\alpha n}\rangle = (\epsilon_\alpha + n\Omega) |\phi_{\alpha n}\rangle, \quad (5)$$

where

$$\hat{H}_F = I \otimes \hat{H}^{(0)} + \sum_{k \in \mathbb{Z}} k\Omega |k\rangle \langle k| \otimes \hat{I} + \sum_{m \in \mathbb{F}} \sum_{k \in \mathbb{Z}} |k+m\rangle \langle k| \otimes \hat{H}^{(m)}, \quad (6)$$

$$|\phi_{\alpha n}\rangle = \sum_{l \in \mathbb{Z}} |l+n\rangle |\phi_\alpha^{(l)}\rangle. \quad (7)$$

Here,  $|l\rangle$  is a basis state of the auxiliary space labeled by the Fourier mode  $l$ , and  $|p\rangle \langle q|$  represents a matrix  $M$  in the auxiliary space in which  $M_{p,q} = 1$ , while all other elements are zero. Also,  $\hat{H}^{(n)}$  is a Fourier component of  $\hat{H}(t)$  and  $\mathbb{F}$  denotes the set of nonzero indices of the Fourier modes corresponding to  $\hat{H}(t)$ . We note that  $\alpha$  denotes a solution within a single Floquet zone, while  $n$  denotes different Floquet zones.

### 1. Simple example of a periodically driven system

In this subsection, we consider an example of a one-qubit driven system to give an explicit expression for the extended Floquet Hamiltonian and discuss the extended Floquet state. The time-periodic Hamiltonian we consider is

$$\hat{H}(t) = d_1 \hat{\sigma}_x + 2d_2 \hat{\sigma}_y \cos(\Omega t) + 2d_3 \hat{\sigma}_z \sin(2\Omega t), \quad (8)$$

where  $d_1, d_2, d_3$  are scalars,  $\Omega = 2\pi/T$ , and  $\hat{\sigma}_x, \hat{\sigma}_y, \hat{\sigma}_z$  are Pauli matrices.

The nonzero Fourier modes of the Hamiltonian are

$$\hat{H}^{(0)} = d_1 \hat{\sigma}_x, \quad \hat{H}^{(1)} = \hat{H}^{(-1)} = d_2 \hat{\sigma}_y, \quad \hat{H}^{(2)} = -\hat{H}^{(-2)} = -id_3 \hat{\sigma}_z.$$

For truncation at five Floquet zones (five-dimensional auxiliary space,  $N_c = 2$ ), Fig. 1(b) schematically shows how the different Fourier modes of the Hamiltonian connect different Fourier modes of the state, or equivalently, different



auxiliary states. The extended Floquet Hamiltonian can be written as

$$\hat{H}_F = \begin{pmatrix} d_1\hat{\sigma}_x - 2\Omega & d_2\hat{\sigma}_y & id_3\hat{\sigma}_z & 0 & 0 \\ d_2\hat{\sigma}_y & d_1\hat{\sigma}_x - \Omega & d_2\hat{\sigma}_y & id_3\hat{\sigma}_z & 0 \\ -id_3\hat{\sigma}_z & d_2\hat{\sigma}_y & d_1\hat{\sigma}_x & d_2\hat{\sigma}_y & id_3\hat{\sigma}_z \\ 0 & -id_3\hat{\sigma}_z & d_2\hat{\sigma}_y & d_1\hat{\sigma}_x + \Omega & d_2\hat{\sigma}_y \\ 0 & 0 & -id_3\hat{\sigma}_z & d_2\hat{\sigma}_y & d_1\hat{\sigma}_x + 2\Omega \end{pmatrix}. \quad (9)$$

This matrix can be decomposed into several terms using auxiliary matrices:

$$\hat{H}_F = \begin{pmatrix} 1 & 0 & 0 & 0 & 0 \\ 0 & 1 & 0 & 0 & 0 \\ 0 & 0 & 1 & 0 & 0 \\ 0 & 0 & 0 & 1 & 0 \\ 0 & 0 & 0 & 0 & 1 \end{pmatrix} \otimes d_1\hat{\sigma}_x + \begin{pmatrix} -2 & 0 & 0 & 0 & 0 \\ 0 & -1 & 0 & 0 & 0 \\ 0 & 0 & 0 & 0 & 0 \\ 0 & 0 & 0 & 1 & 0 \\ 0 & 0 & 0 & 0 & 2 \end{pmatrix} \otimes \hat{I} + \begin{pmatrix} 0 & 1 & 0 & 0 & 0 \\ 1 & 0 & 1 & 0 & 0 \\ 0 & 1 & 0 & 1 & 0 \\ 0 & 0 & 1 & 0 & 1 \\ 0 & 0 & 0 & 1 & 0 \end{pmatrix} \otimes d_2\hat{\sigma}_y + \begin{pmatrix} 0 & 0 & i & 0 & 0 \\ 0 & 0 & 0 & i & 0 \\ -i & 0 & 0 & 0 & i \\ 0 & -i & 0 & 0 & 0 \\ 0 & 0 & -i & 0 & 0 \end{pmatrix} \otimes d_3\hat{\sigma}_z. \quad (10)$$

After diagonalizing  $\hat{H}_F$ , we obtain 10 eigenvalues, corresponding to two quasienergies per Floquet zone. Once the quasienergies in the central Floquet zone are known, neglecting the error due to truncation, the quasienergies in any other Floquet zone can be obtained by shifting the central zone quasienergies by an integer multiple of  $\Omega$ . Since the central Floquet zone contains all the necessary information and provides the most accurate results, it is sufficient to focus on this zone. The extended Floquet states in the central Floquet zone ( $n = 0$ ) are given by

$$(|\phi_\alpha^{(-2)}\rangle, |\phi_\alpha^{(-1)}\rangle, |\phi_\alpha^{(0)}\rangle, |\phi_\alpha^{(1)}\rangle, |\phi_\alpha^{(2)}\rangle)^T, \text{ where } \alpha \in \{0, 1\}.$$

We can express the Floquet states as

$$|\phi_\alpha(t)\rangle = \sum_{l=-2}^2 e^{il\Omega t} |\phi_\alpha^{(l)}\rangle. \quad (11)$$

We note that  $|\phi_\alpha(0)\rangle$  is an eigenstate of  $\hat{H}_F$  with eigenvalue  $\epsilon_\alpha$ . To fully describe the time-periodic Floquet state, we also need to know the micromotion operator  $\hat{\Phi}(t)$ , where  $|\phi_\alpha(t)\rangle = \hat{\Phi}(t) |\phi_\alpha(0)\rangle$ .

When  $d_1$ ,  $d_2$ , and  $d_3$  depend on a parameter or set of parameters  $\vec{k}$ , two quasienergy bands are obtained in each Floquet zone, as shown schematically in Fig. 1(c). In the central Floquet zone, the quasienergies are  $\epsilon_\alpha(\vec{k})$ , and the corresponding extended Floquet state is  $(|\phi_\alpha^{(-2)}(\vec{k})\rangle, |\phi_\alpha^{(-1)}(\vec{k})\rangle, |\phi_\alpha^{(0)}(\vec{k})\rangle, |\phi_\alpha^{(1)}(\vec{k})\rangle, |\phi_\alpha^{(2)}(\vec{k})\rangle)^T$ , where  $\alpha \in \{0, 1\}$ . In solid-state systems,  $\vec{k}$  can be thought of as the crystal momentum.

We emphasize here that there are two distinct approaches to studying quasienergies and Floquet states in periodically driven systems. These are: (i) using the Floquet unitary ( $\hat{U}_F$ ), and (ii) preparing eigenstates of the extended Floquet Hamiltonian. In the case of a continuous periodic drive, obtaining  $\hat{U}_F$  through Trotterization requires a much deeper circuit [35]. In Fig. (2), we schematically show the deeper circuit required to implement  $\hat{U}_F$ , compared to the shallower and wider circuit that results from applying the extended Floquet Hamiltonian framework. Therefore, the extended Floquet Hamiltonian framework is likely to be more efficient for studying quantum many-body systems subject to continuous driving on NISQ devices.

## B. ADAPT-VQE

The ADAPT-VQE algorithm [24] employs a greedy strategy to iteratively construct a variational ansatz using operators from a fixed, user-defined operator pool, starting from an initial state  $|\psi_{\text{ref}}\rangle$ . Let  $\mathcal{O} = \{\hat{O}^{(1)}, \hat{O}^{(2)}, \dots, \hat{O}^{(N)}\}$  be the pool of operators. Then, defining  $\boldsymbol{\theta}^{(k)} = (\theta_1, \dots, \theta_k)$  to be the variational parameters in the ansatz at iteration  $k$ , the ansatz  $|\psi_k(\boldsymbol{\theta}^{(k)})\rangle$  is grown by appending operator  $\hat{O}_{k+1} \in \mathcal{O}$  to it, with a corresponding variational coefficient  $\theta_{k+1}$ , to generate the new ansatz

$$|\psi_{k+1}(\boldsymbol{\theta}^{(k+1)})\rangle = e^{-i\theta_{k+1}\hat{O}_{k+1}} |\psi_k(\boldsymbol{\theta}^{(k)})\rangle. \quad (12)$$

In Eq. (12), the operator  $\hat{O}_{k+1}$  that is appended to the previous ansatz is chosen by measuring the energy gradient of each pool operator  $\left| \partial \langle \hat{H} \rangle / \partial \theta_{k+1} \right|_{\theta_{k+1}=0}$  at the state  $|\psi_k(\boldsymbol{\theta}^{(k)})\rangle$  and selecting the operator that has the largest

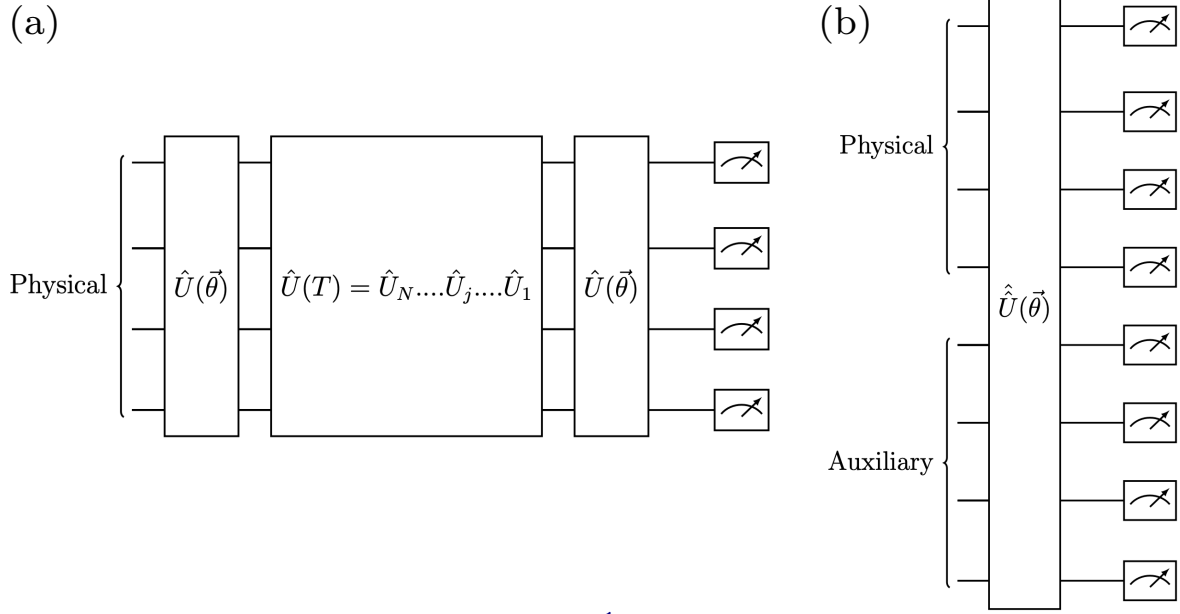


FIG. 2. Schematic diagram of (a) the deeper quantum circuit needed to realize the Floquet unitary ( $\hat{U}_F = \hat{U}(T)$ ) versus (b) the shallower and wider circuit needed for preparing eigenstates of the extended Floquet Hamiltonian.

gradient. The energy gradient of a pool operator can be expressed as

$$\left| \partial \langle \hat{H} \rangle / \partial \theta_{k+1} \Big|_{\theta_{k+1}=0} \right| = \left| \langle \psi_k(\boldsymbol{\theta}^{(k)}) | [\hat{O}_{k+1}, \hat{H}] | \psi_k(\boldsymbol{\theta}^{(k)}) \rangle \right|, \quad (13)$$

where the right hand side of Eq. (13) can be efficiently measured on a quantum processor. A convergence check follows the measurement of the pool operator gradients: If the gradient norm of the pool operators is smaller than a threshold  $\varepsilon$ , the calculation is terminated and declared converged; if not, the ansatz is grown as in Eq. (12). Finally, a VQE optimization of all variational parameters is performed, in which the parameters are initialized as  $\boldsymbol{\theta}_{k+1} : (\theta_1 = \theta_1^*, \dots, \theta_k = \theta_k^*, \theta_{k+1} = 0)$ , i.e., the parameters  $(\theta_1, \dots, \theta_k)$  take their previously optimized values, and the newly added parameter  $\theta_{k+1}$  is initialized to 0. The steps of growing the ansatz and re-optimizing the coefficients are repeated until the convergence criterion is met.

The ADAPT-VQE algorithm was demonstrated to reach arbitrarily accurate energies and yield shallow ansätze in simulations of small molecules [24, 25, 36]. Recently, there have been improvements, including adding operators in batches to further improve circuit compactness, as in the TETRIS-ADAPT-VQE algorithm [26]. It has also been extended to a diverse range of problems beyond chemistry, including ground-state preparation for strongly-correlated systems in high-energy [37, 38] and condensed matter [39, 40] physics, thermal state preparation [41], as well as the calculations of excited states [42], time-evolution [43] and dynamics [44]. Its versatility makes it especially suitable to the task of generating shallow circuits that prepare extended Floquet states.

### III. FLOQUET-ADAPT-VQE ALGORITHM

We begin this section by developing a method to decompose the auxiliary matrices into a Pauli basis to facilitate mapping the extended Floquet Hamiltonian onto a quantum processor. To formulate the Floquet-ADAPT-VQE algorithm, we need to define a cost function, find a suitable initial state, and choose pool operators. This algorithm prepares extended Floquet states on a quantum processor and obtains the full spectrum of quasienergies. Finally, we propose quantum circuit to calculate the expectation value of an operator after an extended Floquet state has been prepared.

### A. Decomposition of auxiliary matrices into Pauli strings

We consider a time-periodic Hamiltonian in a  $D$ -dimensional Hilbert space. For convenience we choose  $D = 2^L$ . In Eq. (6), the extended Floquet Hamiltonian contains an odd number  $(2N_c + 1)$  of Floquet zones and so has an odd-dimensional auxiliary space. However, in order to implement our Hamiltonian on qubit-based quantum hardware, we require the dimension to be a power of 2. For this purpose, we choose the number  $n_a$  of auxiliary qubits and the cut-off  $N_c$  such that  $2(N_c + 1) = 2^{n_a}$ , and arrange the extended Hamiltonian into two blocks. The larger block contains  $2N_c + 1$  Floquet zones and the smaller contains one Floquet zone (see Appendix A). We can write the extended Floquet Hamiltonian as

$$\hat{H}_F = I \otimes \hat{H}^{(0)} + \Omega A^d \otimes \hat{I} + \sum_{r \in \mathbb{F}} (A^{(r)} - A_{\text{asy}}^{(r)}) \otimes \hat{H}^{(r)}, \quad (14)$$

where  $I$  ( $\hat{I}$ ) is the identity matrix in the auxiliary (physical) Hilbert space, and  $A^d = \sum_n n |n\rangle \langle n|$ ,  $A^{(r)} = \sum_n |n+r\rangle \langle n|$  are respectively diagonal and off-diagonal matrices in the auxiliary space, where the summations are over all the states in the auxiliary space for which  $-N_c \leq n \leq N_c + 1$  and  $-N_c \leq n+r \leq N_c + 1$ . In the summation in Eq. (14),  $\mathbb{F}$  denotes the set of indices labeling the nonzero Fourier modes of the time-periodic Hamiltonian. The final term in Eq. (14) involving  $A_{\text{asy}}^{(r)}$  is subtracted to ensure that the extended Floquet Hamiltonian is block-diagonalized and that the larger blocks remain symmetric across the Floquet zones. Here,  $\hat{H}^{(r)}$  is a Fourier mode of the time-periodic Hamiltonian  $\hat{H}(t)$  and belongs to the physical Hilbert space ( $\mathcal{H}$ ).

We decompose the auxiliary diagonal matrix  $A^d$  and off-diagonal matrices  $A^{(r \neq 0)}$  in terms of Pauli strings (matrices). Naively, we could use a trace-based method:

$$A^{(r)} = \sum_{j=1}^{4^{n_a}} d_j P_j, \quad d_j = \frac{1}{2^{n_a}} \text{Tr}[A^{(r)} P_j], \quad (15)$$

where  $P_j \in \{I, X, Y, Z\}^{\otimes n_a}$  and  $\{d_j\}_{j=1}^{4^{n_a}}$  are complex coefficients. However, this approach is not efficient as it requires calculating  $4^{n_a}$  coefficients, while the structure of the auxiliary matrices allows them to be decomposed into a much smaller subset of Pauli strings in which most of the  $4^{n_a}$  coefficients  $d_j$  are in fact zero. We now present the explicit form of these decompositions.

The diagonal auxiliary matrix  $A^d$  can be decomposed into Pauli terms  $P_j \in \{I, Z\}^{\otimes n_a}$  with coefficients  $\{d_j\}$ . Although a generic diagonal matrix has  $2^{n_a}$  such terms, the specific form of  $A^d$  in the extended Floquet Hamiltonian is comprised of only  $n_a + 1$  Pauli strings. In particular, we can write  $A^d = \sum_j d_j Z_{(j)} + \frac{1}{2}I$ , where  $Z_{(j)} = I_{n_a-1} \otimes \cdots \otimes I_{j+1} \otimes Z_j \otimes I_{j-1} \cdots \otimes I_0$ . Here, the coefficients are given by  $d_j = -2^{j-1}$ . For the off-diagonal matrices  $A^{(r \neq 0)}$ , we have

$$A^{(-1)} = \sum_{n=-N_c}^{N_c} |n\rangle \langle n+1| = \sum_{k=0}^{n_a-1} I^{\otimes k} \otimes P^+ \otimes (P^-)^{\otimes n_a-k-1}, \quad (16)$$

$$A^{(1)} = A^{(-1)\dagger} = \sum_{n=-N_c}^{N_c} |n+1\rangle \langle n| = \sum_{k=0}^{n_a-1} I^{\otimes k} \otimes P^- \otimes (P^+)^{\otimes n_a-k-1}, \quad (17)$$

$$A^{(|r|)} = [A^{(1)}]^{|r|}, \quad A^{(-|r|)} = A^{(|r|)\dagger} = [A^{(-1)}]^{|r|}, \quad (18)$$

where  $P^\pm = (X \pm iY)/2$ . The number of Pauli strings in each of these operators is  $O(2^{n_a})$  (see Appendix A1).

For the auxiliary matrices that we use to correct for truncation asymmetries, we find

$$A_{\text{asy}}^{(r>0)} = |N_c + 1\rangle \langle N_c + 1 - r| = (P^-)^{x_{n_a-1}} (Z^-)^{1-x_{n_a-1}} \otimes \cdots \otimes (P^-)^{x_0} (Z^-)^{1-x_0}, \quad (19)$$

$$A_{\text{asy}}^{(r<0)} = |N_c + 1 - |r|| \langle N_c + 1| = (P^+)^{x_{n_a-1}} (Z^-)^{1-x_{n_a-1}} \otimes \cdots \otimes (P^+)^{x_0} (Z^-)^{1-x_0}, \quad (20)$$

where

$$x_i = \left\lfloor \frac{|r|}{2^i} \right\rfloor \mod 2, \quad (21)$$

and  $Z^\pm = (I \pm Z)/2$ . In other words, we first express  $|r|$  as an  $n_a$ -bit string (say,  $r_{\text{bit}}$ ). Then we replace 0 with  $Z^-$  and 1 with  $P^-$  (for  $A_{\text{asy}}^{(r>0)}$ ) or  $P^+$  (for  $A_{\text{asy}}^{(r<0)}$ ) in  $r_{\text{bit}}$ . For example, if  $n_a = 5$  and  $r = 3$ , we have  $r_{\text{bit}} = 00011$  and so  $A_{\text{asy}}^{(3)} = Z^- \otimes Z^- \otimes Z^- \otimes P^- \otimes P^-$ ,  $A_{\text{asy}}^{(-3)} = Z^- \otimes Z^- \otimes Z^- \otimes P^+ \otimes P^+$ . Thus, each asymmetric auxiliary matrix can be decomposed into  $2^{n_a}$  Pauli strings, and we find that the number of Pauli strings needed to express auxiliary matrices is  $O(2^{n_a})$ , which is much less than the total number of Pauli strings ( $4^{n_a}$ ).

For any quantum simulation, converting a Hamiltonian into a sum of Pauli strings is the first and necessary step toward its implementation on a qubit-based quantum processor. Therefore, we would like to emphasize that the Pauli decomposition of the auxiliary matrices and the extended Floquet Hamiltonian serves as a basic input for various algorithms in both near-term and fault-tolerant eras. For example, this decomposition can also be used for simulating quantum dynamics via the time-evolution unitary of the extended Floquet Hamiltonian in the Floquet-Hilbert space [45, 46].

In order to efficiently simulate an  $L$ -qubit time-independent Hamiltonian on a quantum processor, the number of Pauli strings representing the Hamiltonian should scale polynomially with  $L$ . For VQEs, we can efficiently measure the energy expectation value if the scaling of the Pauli strings is polynomial [22]. However, in the case of an extended Floquet Hamiltonian, the number of Pauli strings required to represent auxiliary matrices scales as  $2^{n_a} = 2(N_c + 1)$ . This implies that, even if the Hamiltonian of the physical register contains a polynomial number of Pauli strings, the total number of Pauli strings in the extended Floquet Hamiltonian will scale as  $O(2^{n_a} \times \text{poly}(L))$ . Therefore, to efficiently simulate the extended Floquet Hamiltonian on a quantum computer, the number of Pauli strings in the auxiliary matrices must scale polynomially with the number of physical qubits  $L$ , i.e.,  $2^{n_a} = \text{poly}(L)$ . Fortunately, for scenarios involving only a few Fourier modes [47], accurate truncation of the extended Floquet Hamiltonian is achievable by taking  $n_a = C \log_2(LJ_{\text{max}}/\Omega)$  where,  $J_{\text{max}}$  is the maximum value of local energy parameters and  $C$  is a constant [48]. Thus, higher frequencies and lower values of  $J_{\text{max}}$  require fewer auxiliary qubits, and vice versa. A more rigorous derivation of the auxiliary-qubits ( $n_a$ ) requirement is provided in Ref. [49], where  $n_a = \Theta(\log(\alpha T) + \log \log(1/\varepsilon))$ . Here,  $\varepsilon$  denotes the error tolerance in quasienergy due to truncation,  $T$  is the drive period and  $\alpha = \max\{||H^{(m)}||\}$ , which is proportional to  $LJ_{\text{max}}$ .

### B. Floquet-ADAPT-VQE algorithm for preparing Floquet states

We now describe our Floquet-ADAPT-VQE algorithm for preparing Floquet states and measuring quasienergies on a quantum computer. We must first identify a suitable cost function. The expectation value of the extended Floquet Hamiltonian  $\hat{H}_F$  might seem to be a natural choice. However, a variational algorithm based on such a cost function would target Floquet states corresponding to the lowest Floquet zone that remains when we truncate the auxiliary space, which is where the truncation errors are largest. Since each Floquet zone contains the same quasienergy spectrum up to a constant shift by an integer multiple of  $\Omega$ , it is instead preferable to target the central Floquet zone, where the truncation errors are minimal. This motivates us to consider a cost function that involves the square of the extended Floquet Hamiltonian shifted by a constant  $\lambda$ :

$$C_\lambda(\vec{\theta}) = \langle\langle \psi(\vec{\theta}) | (\hat{H}_F - \lambda \hat{I})^2 | \psi(\vec{\theta}) \rangle\rangle. \quad (22)$$

The shift parameter  $\lambda$  can be chosen to target a quasienergy close to  $\lambda$ , in a manner analogous to similar methods used for solving static problems variationally [50]. We choose  $-\Omega/2 < \lambda < \Omega/2$  to find quasienergies in the central Floquet zone. Here,  $\vec{\theta}$  are the variational parameters at each ADAPT iteration as discussed in Sec. II B, and  $|\psi(\vec{\theta})\rangle$  is the normalized extended Floquet state. The cost function is strictly nonnegative and attains its minimal value when  $|\psi(\vec{\theta})\rangle$  is the Floquet state whose quasienergy is closest to  $\lambda$ . By minimizing the cost function using the ADAPT-VQE algorithm, we thus expect to obtain the quasienergy closest to  $\lambda$  and its corresponding state. We denote  $\vec{\theta}_0 = \text{argmin}(C_\lambda(\vec{\theta}))$  at the final ADAPT iteration. We can test whether the state is the actual Floquet state by taking the expectation value of  $\hat{H}_F$ . If we find that  $\langle\langle \psi(\vec{\theta}_0) | \hat{H}_F | \psi(\vec{\theta}_0) \rangle\rangle \in \{\pm\sqrt{C_\lambda(\vec{\theta}_0)} + \lambda\}$  then we have prepared the extended Floquet state and the quasienergy is  $\langle\langle \psi(\vec{\theta}_0) | \hat{H}_F | \psi(\vec{\theta}_0) \rangle\rangle$ .

Now, we set  $\lambda = 0$  to define the cost function as  $C_0(\vec{\theta})$ . The eigenstates of  $\hat{H}_F^2$  are also eigenstates of  $\hat{H}_F$ , except for cases where quasienergies appear in pairs of  $\pm\epsilon$ . This pairing occurs when  $\hat{H}_F$  exhibits chiral symmetry or particle-hole symmetry, where there exists an operator  $\hat{\Gamma}$  satisfying  $\{\hat{H}_F, \hat{\Gamma}\} = \hat{H}_F \hat{\Gamma} + \hat{\Gamma} \hat{H}_F = 0$ . After minimizing the cost function, we obtain a quantum state and calculate the expectation value of the extended Floquet Hamiltonian  $\hat{H}_F$ . If the expectation value is  $\pm\sqrt{C_0(\vec{\theta}_0)}$ , the extended Floquet state has been prepared. Otherwise, we have a superposition

of extended Floquet states given by  $c_1 |\phi(\vec{\theta}_0)\rangle + c_2 \hat{\Gamma} |\phi(\vec{\theta}_0)\rangle$ , with  $|c_1|^2 + |c_2|^2 = 1$  and  $|\phi\rangle$  is an eigenvector with eigenvalue  $\epsilon$ .

Next, for  $\lambda \neq 0$  the cost function targets a specific quasienergy and Floquet state. Here, even if  $\hat{H}_F$  has chiral symmetry or particle-hole symmetry,  $\hat{H}_F - \lambda \hat{I}$  does not. By choosing a very small value of  $\lambda$ , we can prepare a Floquet state even in the presence of chiral symmetry or particle-hole symmetry. Moreover, by treating  $\lambda$  as a tunable parameter and discretizing it, we can determine the full quasienergy spectrum. To capture all extended Floquet states within the central Floquet zone, we may need to employ a very fine mesh for  $\lambda$ . However, the key advantage of this approach compared to other methods, like the one used in Ref. [28, 51] is that it does not require including additional penalty terms in the cost function to project out previously prepared eigenstates, which significantly increase the measurement costs.

The choice of the initial state significantly affects the convergence of VQE. We focus on targeting quasienergy states in the central Floquet zone ( $0 < \epsilon^2 < \Omega^2/4$ ) since the truncated extended Floquet Hamiltonian provides the most accurate Floquet states within this zone. However, the full spectrum of squared quasienergies extends from zero to  $(N_c + 1/2)^2 \Omega^2$ , where  $N_c$  represents the number of truncated positive Floquet zones. A randomly chosen state is more likely to be further away from the central Floquet zone as we increase  $N_c$  or  $n_a$ . This adversely affects the convergence of a VQE. Therefore, it is crucial to identify an auxiliary state that brings the squared Floquet energy ( $C_0(\vec{\theta})$ ) closer to the central Floquet zone. We choose a state which is an eigenstate of  $A^d$  with zero eigenvalue:

$$|\psi_{\text{in}}\rangle = |0\rangle \otimes |\phi_p\rangle, \quad (23)$$

where  $|0\rangle$  is the auxiliary state associated with the central Floquet zone that satisfies  $A^d |0\rangle = 0$ , and where  $|\phi_p\rangle$  is an initial state of the physical system. In the standard basis of  $\mathbb{R}^{2^{n_a}}$  in which  $|-N_c\rangle$  is represented as  $(1, 0, \dots, 0)^T$ , this auxiliary state is  $|0\rangle \equiv (0, \dots, 0, 1, 0, \dots, 0)^T$ , where there is a single 1 in the  $2^{n_a-1}$ th component. In the computational basis of the  $n_a$ -qubit auxiliary space in which  $|-N_c\rangle \equiv |\uparrow_{n_a-1} \uparrow_{n_a-2} \dots \uparrow_1 \uparrow_0\rangle$ ,  $|0\rangle \equiv |\uparrow_{n_a-1} \downarrow_{n_a-2} \dots \downarrow_1 \downarrow_0\rangle$ , where  $|\uparrow\rangle \equiv (1 \ 0)^T$ ,  $|\downarrow\rangle \equiv (0 \ 1)^T$ . The cost function value for this choice of auxiliary initial state is independent of the number of auxiliary qubits  $n_a$ , as well as the frequency  $\Omega$  (see Appendix B for a proof), thereby keeping the energy of the initial state close to or within the central Floquet zone for arbitrary truncation and driving frequency. Further improvements to the initial state can be made by optimizing the choice of  $|\phi_p\rangle$  based on the specific physical system under consideration.

To run Floquet-ADAPT-VQE, we need to define an operator pool that aids in creating the ansatz in a problem-informed manner. The simplest (though not necessarily the most efficient) choice for the operator pool is the standard pool of Pauli strings used for a static system with  $L + n_a$  qubits. However, for systems that require more auxiliary qubits, this might lead to an unreasonable number of gradient measurements. To prevent this, we construct a mixed Floquet pool by using different operator pools for the auxiliary and physical parts of the Floquet-Hilbert space. For example, we might select the full Pauli pool for the auxiliary part and a pool of two-local operators for the physical part in the case of a spin-lattice system. Depending on the type of physical system, various operator pools can be chosen based on existing works on static Hamiltonians [25, 40, 52, 53]. We summarize the full Floquet-ADAPT-VQE algorithm in Algorithm 1.

---

#### Algorithm 1 Floquet-ADAPT-VQE

---

**Input:** Fourier modes of the time-periodic Hamiltonian

**Output:** Quasienergies and Floquet state in Floquet-Hilbert space prepared on a quantum processor

1. Construct all the auxiliary operators  $A^{(r)}$  and construct  $\hat{H}_F^2$  in the Floquet-Hilbert space
  2. Choose an initial state as  $|\psi_{\text{in}}\rangle = |0\rangle \otimes |\phi_p\rangle$
  3. Select Floquet operator pools (a mix of auxiliary and physical pools) in Floquet-Hilbert space
  4. Apply the ADAPT-VQE subroutine on  $\hat{H}_F^2$  to obtain the Floquet state and squared quasienergies closest to zero
  5. To obtain the full quasienergy spectrum within the central Floquet zone, discretize  $\lambda$  finely and apply the ADAPT-VQE subroutine on  $(\hat{H}_F - \lambda \hat{I})^2$ . Adjust the initial state as needed to capture the full spectrum
  6. To find the exact quasienergy, compute the expectation value of  $\hat{H}_F$  in the Floquet state
- 

### C. Expectation value of operator in Floquet state in time

Now we provide an algorithm to calculate the expectation value of an operator  $\hat{O}$  evolving in time using the extended Floquet state. We can write the expectation value in the extended Floquet-Hilbert space as (see Appendix C for details)

$$\langle \hat{O}(t) \rangle_\phi = \langle \phi(t) | \hat{O} | \phi(t) \rangle = \langle \langle \phi | \hat{U}^\dagger(t) \hat{O} \hat{U}(t) | \phi \rangle \rangle, \quad (24)$$



where  $\hat{U}(t) = e^{iA^d \Omega t} \otimes \hat{I}$  such that  $A^d$  is the diagonal auxiliary matrix and  $\hat{O} = A_o \otimes \hat{O}$ , where  $A_o$  is a real matrix with all elements being one [see Appendix C]. For an  $n_a$ -qubit auxiliary space,  $e^{iA^d \Omega t} = e^{i\Omega t/2} \otimes_j R_j^z(\Omega t)$ , and  $R_j^z(\Omega t) = e^{-i(2^{j-1}\Omega t)Z_j}$  is a single qubit  $Z$ -rotation operator and  $j \in \{0, 1, \dots, n_a - 1\}$ . The tensor product is ordered such that the  $j = n_a - 1$  operator is the left-most, and the  $j = 0$  operator is the right-most. For  $\hat{O} = A_o \otimes \hat{O}$ , we can express  $A_o$  in terms of all possible products of Pauli  $X$  and identity  $I$  as  $A_o = (I + X)^{\otimes n_a} = \sum_{j=0}^{2^{n_a}-1} P_j$  such that  $P_j \in \{I, X\}^{\otimes n_a}$ . We note that all the coefficients are equal to one in this summation of Pauli operators. We can further simplify the expectation value of an operator:

$$\begin{aligned}
 \langle \hat{O}(t) \rangle_\phi &= \langle \phi | \hat{U}^\dagger(t) \hat{O} \hat{U}(t) | \phi \rangle \\
 &= \langle \phi | [\otimes_j R_j^z(-\Omega t)] \otimes \hat{I} (A_o \otimes \hat{O}) [\otimes_j R_j^z(\Omega t)] \otimes \hat{I} | \phi \rangle \\
 &= \langle \tilde{\phi}(t) | A_o \otimes \hat{O} | \tilde{\phi}(t) \rangle \\
 &= \langle \tilde{\phi}(t) | (I + X)^{\otimes n_a} \otimes \hat{O} | \tilde{\phi}(t) \rangle,
 \end{aligned} \tag{25}$$

where  $|\tilde{\phi}(t)\rangle = [\otimes_j R_j^z(\Omega t)] \otimes \hat{I} |\phi\rangle$ . Thus, to measure the physical operator  $\hat{O}$ , we need to first apply time-dependent  $Z$ -rotations to the auxiliary qubits. We then measure  $I + X$  on each of the auxiliary qubits, and we measure  $\hat{O}$  on the physical qubits. When we consider  $t = nT$ , then the stroboscopic expectation value is

$$\langle \hat{O}(nT) \rangle_\phi = \langle \phi | (I + X)^{\otimes n_a} \otimes \hat{O} | \phi \rangle, \tag{26}$$

and so the time-dependent  $Z$ -rotations are not needed in this case; instead we can measure  $(I + X)^{\otimes n_a} \otimes \hat{O}$  directly on the extended Floquet state. At all other times, we must first apply  $Z$ -rotations to the auxiliary qubits before making the measurements. We see that measuring the expectation value of an operator is simplified by the fact that all the terms in  $A_o = (I + X)^{\otimes n_a}$  bit-wise commute. Thus we can measure each auxiliary qubit in the  $X$ -basis, and there is no need for basis transformations involving entangling gates in the auxiliary space. We can measure  $\hat{O}$  on the physical qubits using the standard procedure of first decomposing this operator in a Pauli basis and then measuring each term. Strategies for grouping Pauli strings into commuting sets can be used to reduce the total measurement count [54–57]. We show the quantum circuit to calculate the expectation value of an operator in Fig. 3.

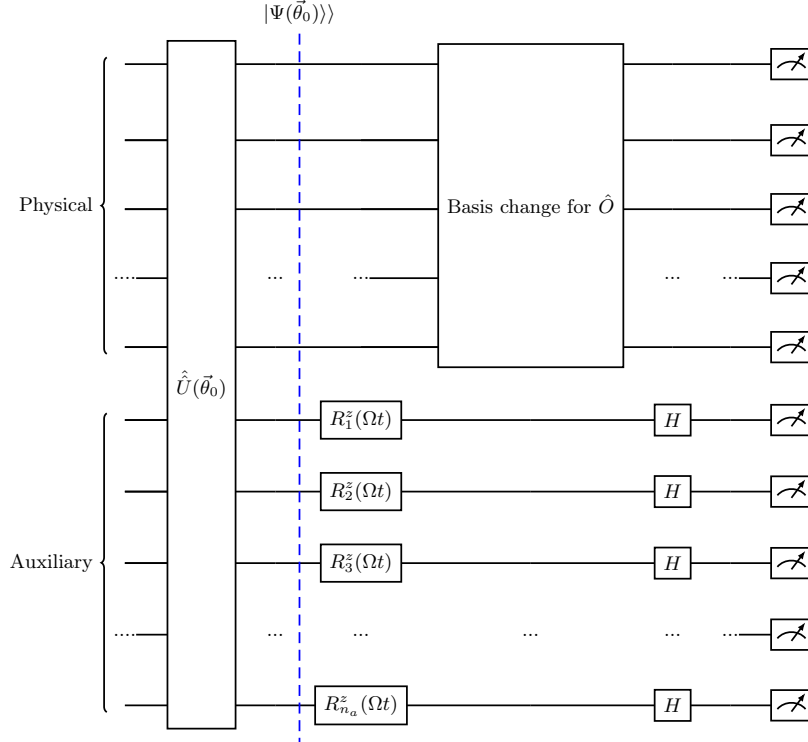


FIG. 3. Quantum circuit to calculate expectation value of an operator  $\hat{O}$  in time using the extended Floquet state.

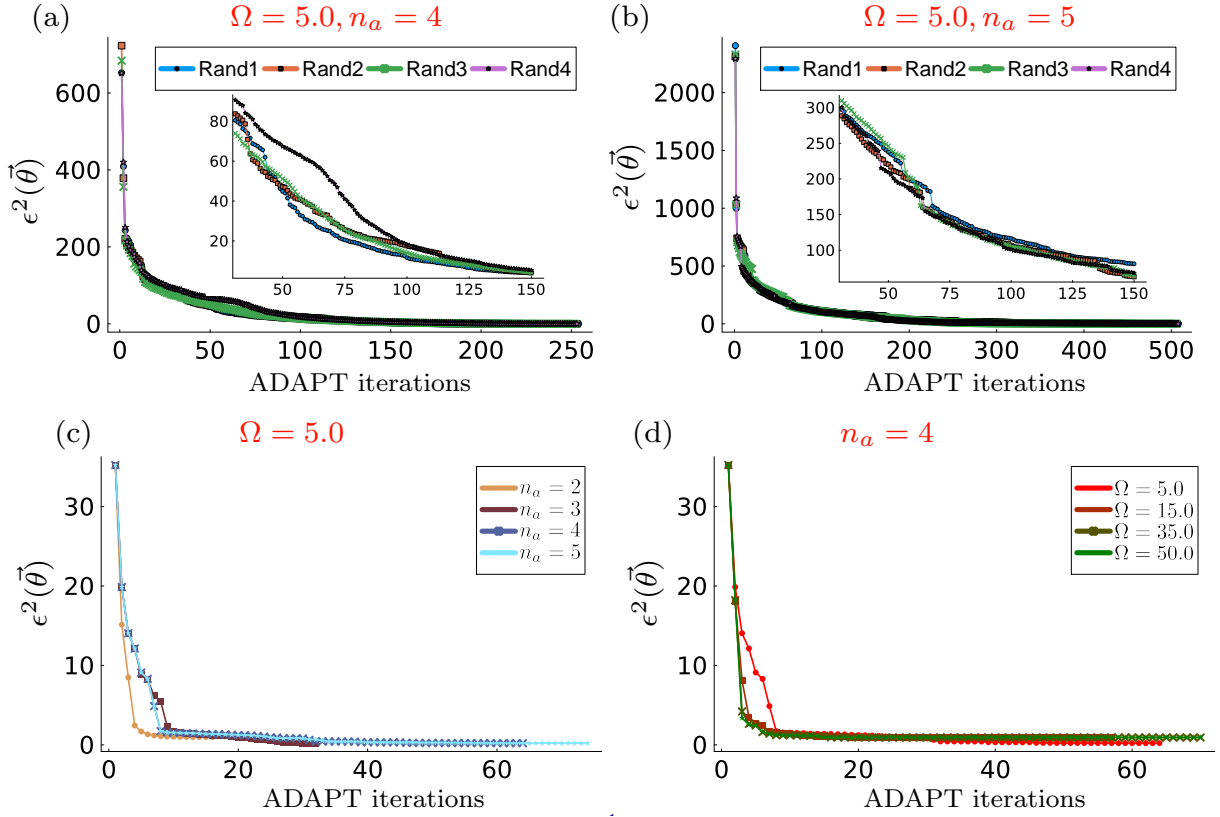


FIG. 4. Squared Floquet energy,  $\epsilon^2(\vec{\theta})$ , of a periodically driven XYZ spin chain with magnetic field as a function of ADAPT iterations for various parameters. All parameters are expressed in units of the characteristic coupling constant  $J_0$ . The squared Floquet energy is shown for four random initial states (as written in the legends) for  $\Omega = 5.0J_0$  and (a)  $n_a = 4$  and (b)  $n_a = 5$ , respectively. The insets provide a closer look at the behavior from iterations 31 to 150. (c) The squared Floquet energy for four different values of  $n_a$  at  $\Omega = 5.0J_0$ . (d) The squared Floquet energy for four different values of  $\Omega$  at  $n_a = 4$ . In both (c) and (d), the initial state is  $|\psi\rangle = |0\rangle \otimes |\phi_p\rangle$ , where  $|\phi_p\rangle = |\downarrow\rangle^{\otimes L}$ . The rest of the parameters are  $L = 3$ ,  $(\bar{J}_x, \bar{J}_y, \bar{J}_z) = (3.7, 2.8, 3.9)J_0$ ,  $(\delta J_x, \delta J_y, \delta J_z) = (0.0, 0.0, 0.0)J_0$ ,  $\bar{B}_z = 2.9J_0$ ,  $\delta B_z = 2.7J_0$ . The couplings and magnetic field values are chosen arbitrarily aside from the conditions that they are of the same order of magnitude and do not exhibit any special relations. Other generic choices of parameters yield similar results. We use a mixed Floquet operator pool consisting of all possible Pauli operators on the auxiliary qubits and two-local XYZ operators on the physical qubits.

We emphasize that this method of calculating time-dependent expectation values is applicable to both near-term and fault-tolerant quantum computers, provided there is a method to prepare the extended Floquet state on the quantum computer. Additionally, this method of calculating the time-dependent expectation value in a Floquet state requires only a fixed-depth circuit, irrespective of the time within a period. In contrast, if we were to prepare a Floquet state  $|\phi(0)\rangle$  in the physical (or original) Hilbert space and use it to compute the time-dependent expectation value  $\langle\phi(0)|\hat{U}^\dagger(t)\hat{O}\hat{U}(t)|\phi(0)\rangle$ , we have to rely on Trotterization for  $\hat{U}(t)$ . In this case, the circuit depth increases as the time within the period increases.

#### IV. NUMERICAL SIMULATION OF DRIVEN XYZ MODEL USING FLOQUET ADAPT-VQE

We now apply Floquet-ADAPT-VQE to study non-equilibrium physics in an XYZ spin chain with periodically driven couplings and with a time-periodic magnetic field. Both the couplings and the magnetic field are taken to have the same period  $T = 2\pi/\Omega$ . The Hamiltonian is

$$H(t) = \sum_{j=1}^{L-1} \left( J_x(t)X_jX_{j+1} + J_y(t)Y_jY_{j+1} + J_z(t)Z_jZ_{j+1} \right) + \sum_{j=1}^L B_z(t)Z_j, \quad (27)$$

where

$$\begin{aligned} J_\mu(t) &= \bar{J}_\mu + \delta J_\mu \cos(\Omega t), \\ B_z(t) &= \bar{B}_z + \delta B_z \cos(\Omega t), \end{aligned} \quad (28)$$

and  $\mu \in \{x, y, z\}$ . The Fourier components of the Hamiltonian are

$$H^{(0)} = \sum_{j=1}^{L-1} \left( \bar{J}_x X_j X_{j+1} + \bar{J}_y Y_j Y_{j+1} + \bar{J}_z Z_j Z_{j+1} \right) + \sum_{j=1}^L \bar{B}_z Z_j, \quad (29)$$

$$H^{(1)} = \sum_{j=1}^{L-1} \frac{1}{2} \left( \delta J_x X_j X_{j+1} + \delta J_y Y_j Y_{j+1} + \delta J_z Z_j Z_{j+1} \right) + \sum_{j=1}^L \frac{1}{2} \delta B_z Z_j. \quad (30)$$

Here,  $H^{(1)} = H^{(-1)\dagger} = H^{(-1)}$ . The extended Floquet Hamiltonian is given by

$$\hat{H}_F = I \otimes \hat{H}^{(0)} + \Omega(A^d \otimes \hat{I}) + (A^{(1)} + A^{(-1)}) \otimes \hat{H}^{(1)} - (A_{\text{asy}}^{(1)} + A_{\text{asy}}^{(-1)}) \otimes \hat{H}^{(1)}. \quad (31)$$

Before presenting the results of our simulations, we define the notation used in this section. The ADAPT quasienergy is defined as  $\epsilon = \langle\langle \psi(\vec{\theta}_0) | \hat{H}_F | \psi(\vec{\theta}_0) \rangle\rangle$ , where  $|\psi(\vec{\theta}_0)\rangle$  is an eigenstate of  $\hat{H}_F^2$  obtained using Floquet-ADAPT-VQE. Additionally, we use the term “squared Floquet energy” to refer to  $\epsilon^2(\vec{\theta}) = \langle\langle \psi(\vec{\theta}) | \hat{H}_F^2 | \psi(\vec{\theta}) \rangle\rangle$ , where  $|\psi(\vec{\theta})\rangle$  is a state in the Floquet-Hilbert space at each ADAPT iteration. We compare the results of the Floquet-ADAPT-VQE algorithm with those obtained by the exact diagonalization (ED) of  $\hat{U}_F$ , not with the ED of the extended Floquet Hamiltonian  $\hat{H}_F$ . We do not use the ED of  $\hat{H}_F$  because it is already approximate due to truncation. In our ED calculation, the eigenvalues  $\epsilon_\alpha$  are obtained from  $\hat{H}_F = (-i/T) \log(\hat{U}_F)$ , and we refer to them as the exact quasienergies. The time evolution operator  $\hat{U}(t)$  and the Floquet unitary  $\hat{U}_F = \hat{U}(T)$  are computed using Trotterization. We use the L-BFGS optimizer to obtain our Floquet-ADAPT-VQE results. Finally, in all that follows, the static and driving coupling parameters, as well as the magnetic fields, are expressed in the same units as the driving frequency. We will express all parameters in units of the characteristic coupling constant  $J_0$ .

Figure 4 highlights the utility of selecting the auxiliary state as the eigenstate corresponding to the zero eigenvalue of the diagonal auxiliary matrix  $A^d$ . The figure shows the squared Floquet energy as a function of the number of ADAPT iterations. In Figs. 4(a) and (b), we consider four random states for  $n_a = 4$  and  $n_a = 5$ , respectively, at a driving frequency of  $\Omega = 5.0J_0$ . The insets zoom in to show finer variations in squared energy over a portion of the ADAPT iterations. We observe that increasing  $n_a$  results in a higher initial squared Floquet energy, which affects the convergence rate. Similarly, in Appendix B we show that increasing  $\Omega$  also leads to a higher initial squared Floquet energy. In Figs. 4(c) and (d), we choose the initial auxiliary state to be the eigenstate of  $A^d$  with zero eigenvalue. In Fig. 4(c), for a fixed driving frequency, we vary  $n_a$  and observe that the initial squared Floquet energy does not depend on  $n_a$ . Similarly, varying the driving frequency in Fig. 4(d), we see that the initial squared Floquet energy does not depend on the driving frequency either. These plots numerically confirm our proof, as discussed in Section III B and Appendix B, that choosing the initial auxiliary state as the eigenstate of  $A^d$  with zero eigenvalue ensures that the initial squared energies are independent of  $n_a$  and  $\Omega$ , leading to better convergence compared to using a random state. This choice of initial state becomes particularly important when studying larger systems at moderate or low driving frequencies, as these regimes require a larger number of auxiliary qubits.

Figure 5 shows the quasienergies for different driving parameters at both moderate  $O(\Omega) \approx O(\delta B, \delta J)$  and high driving frequencies ( $\Omega \gg \delta B, \delta J$ ). Each panel includes an inset that displays the relative error in the quasienergy compared to the ED solution. Figures 5(a) and (b) show the variation in quasienergies with respect to the driven magnetic field for static coupling terms. In Fig. 5(a), we consider a moderate frequency ( $\Omega = 5.0J_0$ ) with  $n_a = 4$  and observe that the Floquet-ADAPT-VQE quasienergies closely match the exact quasienergies, particularly at lower driving amplitudes. As the driving amplitude increases, the relative error also increases, suggesting that a higher number of auxiliary qubits is needed for improved accuracy. In Fig. 5(b), we examine a high frequency ( $\Omega = 50.0J_0$ ) with  $n_a = 3$  and find that the Floquet-ADAPT-VQE and exact quasienergies are very close. Although the relative error does increase with the increase in amplitude, it remains well within acceptable limits for most applications. In Figs. 5(c) and (d), we consider the effects of driving terms in both the coupling and magnetic field. Here, we fix the driving amplitude of the magnetic field and vary the amplitude of the coupling terms. In Fig. 5(c), we analyze the variation in the quasienergy at a moderate frequency ( $\Omega = 5.0J_0$ ) with  $n_a = 4$ , while in Fig. 5(d), we examine it in the high-frequency limit ( $\Omega = 50.0J_0$ ) with  $n_a = 3$ . The results in these cases are qualitatively similar to those observed when only the magnetic field is driven. These figures demonstrate that systems with higher driving frequencies require fewer auxiliary qubits, while systems with lower frequencies need more auxiliary qubits for improved accuracy.

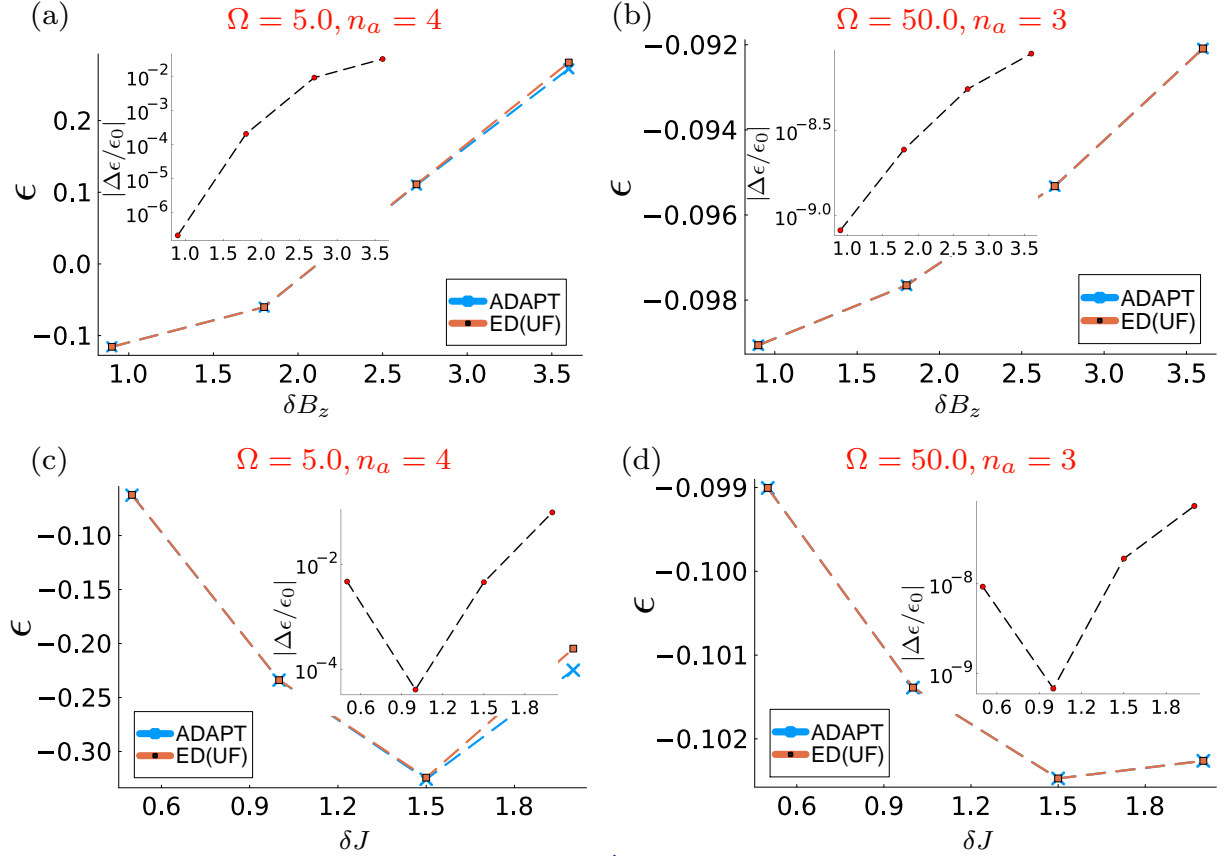


FIG. 5. The quasienergies  $\epsilon = \langle\langle\psi_0|\hat{H}_F|\psi_0\rangle\rangle$  obtained using Floquet-ADAPT-VQE (“ADAPT”) as well as the exact quasienergies (“ED(UF)”) as a function of drive parameters in a periodically driven XYZ spin chain with a magnetic field. All parameters are expressed in units of the characteristic coupling constant  $J_0$ . The insets provide the relative error ( $|\Delta\epsilon/\epsilon_0| = |(\epsilon - \epsilon_0)/\epsilon_0|$ ) of the Floquet-ADAPT-VQE quasienergies with respect to the exact quasienergies. (a,b) The quasienergies versus the driving amplitude of the magnetic field  $\delta B_z$  when the couplings  $J$  are static, i.e.,  $(\delta J_x, \delta J_y, \delta J_z) = (0.0, 0.0, 0.0)J_0$ . In (a), we take  $\Omega = 5.0J_0$  and  $n_a = 4$  and in (b)  $\Omega = 50.0J_0$ ,  $n_a = 3$ . (c,d) The quasienergies with drive terms applied to both the couplings and magnetic field, where the magnetic field amplitude is fixed at  $\delta B_z = 2.7J_0$  and the driven coupling terms are  $(\delta J_x, \delta J_y, \delta J_z) = \delta J \times (1.9, 1.1, 1.2)J_0$ . In (c),  $\Omega = 5.0J_0$  and  $n_a = 4$  and in (d)  $\Omega = 50.0J_0$ ,  $n_a = 3$ . The rest of the parameters for all panels are  $L = 4$ ,  $(\bar{J}_x, \bar{J}_y, \bar{J}_z) = (3.7, 2.8, 3.9)J_0$ ,  $\bar{B}_z = 2.9J_0$ . The initial state is  $|\psi_{\text{in}}\rangle = |0\rangle \otimes |\phi_p\rangle$ , where  $|\phi_p\rangle = |+\rangle^{\otimes L}$ . We use a mixed Floquet operator pool consisting of all possible Pauli operators on the auxiliary qubits and two-local XYZ operators on the physical qubits.

Additionally, it is worth noting that results like those shown in Figs. 5(a) and (c) cannot be simulated accurately using the extended space method from Ref. [28] due to its limited truncation capacity.

In Fig. 6, we present the quasienergy spectrum in the central Floquet zone for the driven XYZ model with magnetic field obtained using numerical simulations of the Floquet-ADAPT-VQE algorithm. The dashed horizontal lines in the figure represent the exact quasienergies within the central Floquet zone. We use  $\lambda$  as a tunable parameter in the cost function, Eq. (22), and discretize its values as  $\lambda \in \{(j - 2^{L+1})\Omega/2^{L+2}\}_{j=1}^{2^{L+2}-1}$ . We begin by selecting the initial state  $|\psi_1\rangle = |0\rangle \otimes |+\rangle^{\otimes 3}$  and calculate the Floquet-ADAPT-VQE quasienergies for the discretized values of  $\lambda$ . The blue line in the figure, representing the quasienergies for this case, captures all but one quasienergy at  $\epsilon = -0.98375J_0$ . Next, we choose a different initial state,  $|\psi_2\rangle = |0\rangle \otimes |\downarrow\rangle^{\otimes 3}$ , and again calculate the Floquet-ADAPT-VQE quasienergies. This time, only half of the full quasienergies are captured, but it successfully identifies the quasienergy that was missed with the previous initial state. We also note that in larger systems, where ED is not feasible, we may not know the specific locations of the missing quasienergies, but we can always determine how many are missing within the central Floquet zone. By finely discretizing  $\lambda$ , varying the initial state, and choosing the pool of operators wisely, we aim to obtain the full quasienergy spectrum. The primary advantage of this method is that each quasienergy calculation is independent of the others, leading to a reduced circuit depth compared to most excited-state VQE methods. In Appendix D, we use the Variational Quantum Deflation algorithm [51] and plot the resultant quasienergies.

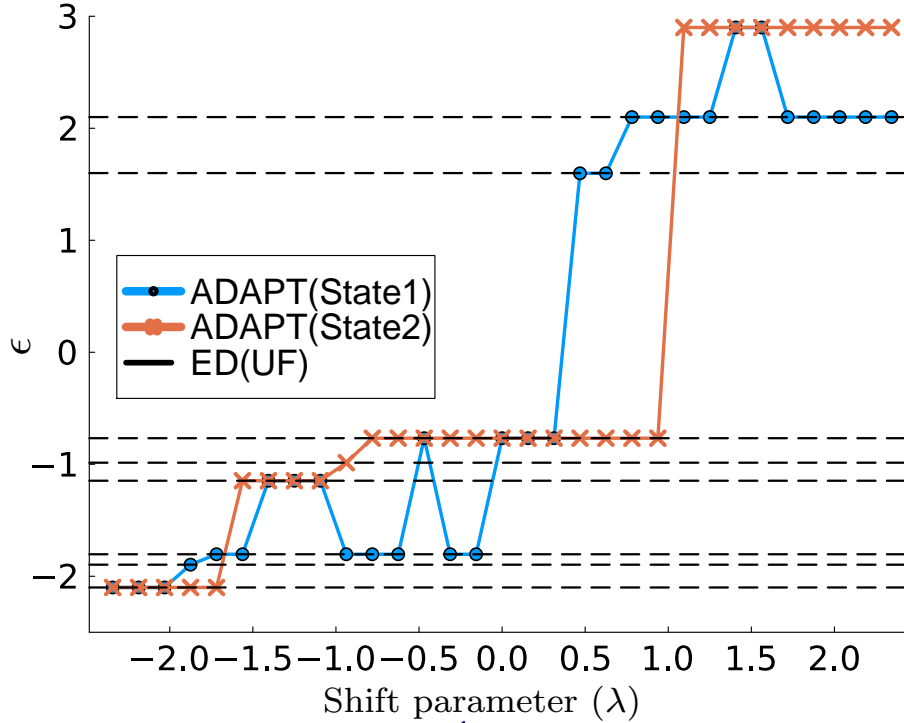


FIG. 6. Quasienergy spectrum of a periodically driven XYZ spin chain as a function of the shift parameter  $\lambda$  in the cost function. All parameters are expressed in units of the characteristic coupling constant  $J_0$ . The dashed lines show the exact quasienergies labeled by ED(UF). The State1 =  $|\psi_1\rangle$  and State2 =  $|\psi_2\rangle$  represent two initial states for the Floquet-ADAPT-VQE algorithm defined as  $|\psi_1\rangle = |0\rangle \otimes |\downarrow\rangle^{\otimes L}$  and  $|\psi_2\rangle = |0\rangle \otimes |+\rangle^{\otimes L}$ . The rest of the parameters are  $L = 3, n_a = 4, (\bar{J}_x, \bar{J}_y, \bar{J}_z) = (3.7, 2.8, 3.9)J_0, (\delta J_x, \delta J_y, \delta J_z) = (1.9, 1.1, 1.2)J_0, B_z = 2.9J_0, \delta B_z = 2.7J_0$ , and  $\Omega = 5.0J_0$ . We use a mixed Floquet operator pool consisting of all possible Pauli operators on the auxiliary qubits and two-local XYZ operators on the physical qubits.

Figure 7 shows the expectation values of two operators. In Fig. 7(a), we show the expectation value of the magnetization ( $\sum_j Z_j$ ), while Fig. 7(b) shows the expectation value of the two-point spin-Z operator ( $\sum_j Z_j Z_{j+1}$ ). These calculations were performed using the algorithms developed in this paper. We first employed Floquet-ADAPT-VQE to prepare the extended Floquet state, then used our algorithm to calculate the expectation values in the Floquet-Hilbert space. For comparison, we also computed the exact time evolution of the operators by applying Trotterization to the time evolution operator  $\hat{U}(t)$  over one period. Both methods produce identical results, clearly demonstrating the periodic nature of the expectation values.

## V. CONCLUSIONS AND OUTLOOK

In this work, we presented a general framework for studying periodically driven many-body quantum systems on a digital quantum processor. We leveraged the Floquet-Hilbert space—a composite vector space comprised of auxiliary and physical spaces—to make the Hamiltonian time-independent. We showed how to map this Hamiltonian in terms of Pauli strings to implement it on a quantum processor. We introduced a hybrid algorithm that we call Floquet-ADAPT-VQE. We defined a cost function based on the square of the shifted, extended Floquet Hamiltonian, enabling us to prepare the extended Floquet state and identify quasienergies anywhere within a Floquet zone. A randomly chosen initial state will typically have low overlap with the target state, leading to less efficient convergence. To address this, we demonstrated how choosing an initial state on the auxiliary register as an eigenstate of a diagonal auxiliary matrix with zero eigenvalue is a good starting point, independent of the number of auxiliary qubits and the driving frequency. Additionally, we provided a protocol for calculating the expectation value of an operator in a Floquet state.

To showcase the utility of Floquet-ADAPT-VQE, we performed classical numerical simulations of our algorithm applied to a periodically driven XYZ spin chain with a magnetic field. Our simulations numerically verified our assertion that the squared Floquet energy of a random initial state remains significantly above the desired Floquet



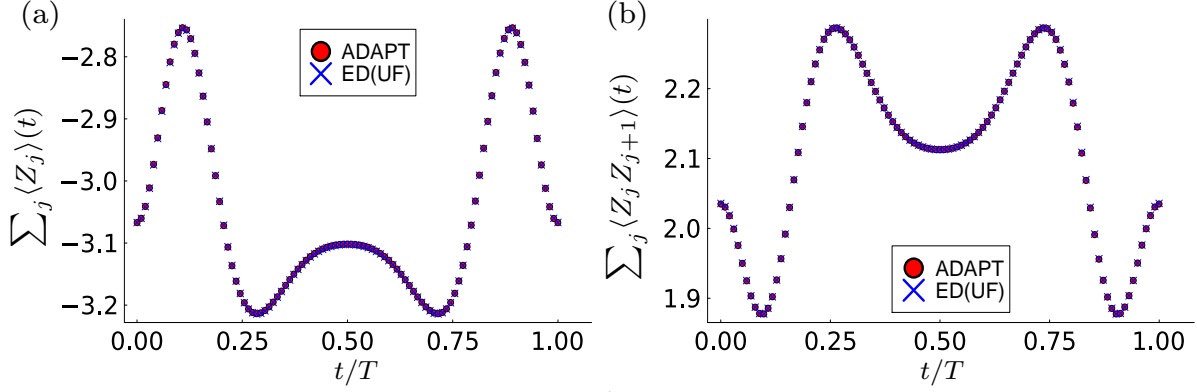


FIG. 7. Expectation values of operators with respect to a Floquet state as a function of time, calculated using Floquet-ADAPT-VQE and direct Trotterization of  $\hat{U}(t)$ . All parameters are expressed in units of the characteristic coupling constant  $J_0$ . (a) The expectation value of the operator  $\sum_j Z_j$ . (b) The expectation value of  $\sum_j Z_j Z_{j+1}$ . Results for both expectation values are shown over one driving period. For the Floquet-ADAPT-VQE calculation, we numerically simulate the algorithm to compute the expectation value of an operator in the extended Floquet state. The extended Floquet state is obtained numerically using Floquet-ADAPT-VQE. The rest of the parameters are  $L = 4$ ,  $(\bar{J}_x, \bar{J}_y, \bar{J}_z) = (3.7, 2.8, 3.9)J_0$ ,  $(\delta J_x, \delta J_y, \delta J_z) = (1.9, 1.1, 1.2)J_0$ ,  $\bar{B}_z = 2.9J_0$ ,  $\delta B_z = 2.7J_0$ . The initial state is  $|\psi_{\text{in}}\rangle = |0\rangle \otimes |\phi_p\rangle$ , where  $|\phi_p\rangle = |+\rangle^{\otimes L}$ . We use a mixed Floquet operator pool consisting of all possible Pauli operators on the auxiliary qubits and two-local XYZ operators on the physical qubits.

zone ( $0 < \epsilon^2 < \Omega^2/4$ ) as the number of the auxiliary qubits and driving frequency increase, leading to a slower convergence of the algorithm. In contrast, the squared Floquet energy of our carefully chosen initial state remains independent of the auxiliary qubits and driving frequency, resulting in better convergence and fewer Floquet-ADAPT-VQE iterations. We also examined how the quasienergies depend on the driving amplitude at both high and moderate frequencies. Furthermore, we calculated the full quasienergy spectrum of the central Floquet zone by scanning over the shift parameter  $\lambda$  in the cost function. Finally, we calculated the expectation value of the net magnetization ( $\sum_j Z_j$ ) and the sum of the two-point  $Z$ -operator ( $\sum_j Z_j Z_{j+1}$ ) in a Floquet state using our algorithms, confirming the efficacy of our protocol for computing expectation values in a Floquet state.

We would like to emphasize that although we used a driven XYZ Hamiltonian as an example, our algorithm is applicable to any type of time-periodic Hamiltonian, including fermionic Hamiltonians. The algorithm is based on transforming a periodic Hamiltonian into an extended Floquet Hamiltonian, which provides a time-independent description that is approximate when a finite number of auxiliary qubits is used. With an arbitrary number of auxiliary qubits, we can approximate any type of periodically driven system. However, with a limited number of auxiliary qubits, the approximation is most effective for systems with a continuous periodic drive featuring a few frequency modes and operating at moderate to high frequencies. Consequently, we believe that our algorithm will be particularly useful for studying phenomena related to light-matter interactions in many-body quantum systems.

Although our study primarily focuses on Floquet-ADAPT-VQE, some of the results obtained in this paper have broader applications across various types of quantum simulation methods. For example, choosing an initial auxiliary state as an eigenstate of the diagonal auxiliary matrix with a zero eigenvalue can reduce the number of convergence steps in any variational algorithm where the cost function is defined using extended Floquet Hamiltonian. Moreover, the Pauli decomposition of auxiliary matrices can be beneficial for any quantum simulation that uses the extended Floquet Hamiltonian. This could also be used for simulating quantum dynamics for a time periodic Hamiltonian [45] like studying dynamics to light driven matter [58]. Additionally, our protocol for calculating the expectation value of an operator can be applied to any gate-based quantum computer once the extended Floquet state is prepared.

Before concluding, we briefly outline two phenomena that could be explored in future studies using our formalism. First, our approach can be used to detect time crystal behavior in a system. The eigenstates of the Floquet unitary in time crystals are long-range correlated states that come in pairs (in the case of period-doubled time crystals), with a quasienergy difference of  $\Omega/2$ . After finding the first eigenstate ( $\epsilon_0 < 0$ ) using Floquet-ADAPT-VQE, the corresponding pair can be identified by tuning  $\lambda = \epsilon_0 + \Omega/2$ . Additionally, our algorithm can also be employed to calculate the stroboscopic time evolution of an operator in the case of a time crystal. More details can be found in Appendix E.

Secondly, we can study phenomena related to light-matter interactions in many-body systems. This algorithm is suitable for simulating multi-frequency light-matter interactions in such systems. By leveraging the extended Floquet state, we can investigate the linear response in periodically driven many-body interacting systems, similar to the

theoretical studies conducted in non-interacting tight-binding Hamiltonians [59]. Furthermore, this approach can be applied to study high harmonic generation in many-body interacting solids [60].

In conclusion, our work establishes a foundation for developing future quantum simulation algorithms for time-periodic systems using the extended Floquet Hamiltonian. Specifically, our Floquet-ADAPT-VQE algorithm facilitates the determination of quasienergies and the preparation of Floquet states within the Floquet-Hilbert space, thereby advancing the study of non-equilibrium physics in periodically driven many-body systems on quantum processors. To implement our algorithm on NISQ devices, further efforts are required to identify more efficient (smaller) operator pools and to study the algorithm's performance under various noise models, which we leave for future work.

## VI. DATA AVAILABILITY

The code and data used to generate the simulations and figures can be found at [https://github.com/AbhiPhy2020/Floq\\_ADAPT\\_v1.jl](https://github.com/AbhiPhy2020/Floq_ADAPT_v1.jl), and make use of the ADAPT-VQE code available at <https://github.com/kmsherbertvt/publiccopy-bp-mitigation-code>. The code requires NLOpt version 0.65. The Exact Diagonalization code can be found at [https://github.com/AbhiPhy2020/Floq\\_ED\\_v0.jl](https://github.com/AbhiPhy2020/Floq_ED_v0.jl).

## ACKNOWLEDGMENTS

A.K. and K.S. would like to thank Samantha Barron and Kyle Sherbert for their helpful comments and discussion on ADAPT-VQE code. K. S. and S. E. E. were supported by the U.S. Department of Energy, Office of Science, National Quantum Information Science Research Centers, Co-design Center for Quantum Advantage (C<sup>2</sup>QA) under Contract No. DE-SC0012704. E.B. and N.M. acknowledge support by the U.S. Department of Energy, Office of Science, Office of Advanced Scientific Computing Research, under Award Number DE-SC0025430.

## Appendix A: Extended Floquet Hamiltonian

As described in the main text, the block-diagonalized extended Floquet Hamiltonian lives in a total space that includes the physical space and an  $n_a$ -qubit auxiliary space. We choose the Fourier indices to range from  $-N_c$  to  $N_c + 1$ . Here is an example of an extended Floquet Hamiltonian in the case of a three-qubit auxiliary space and for a driving term that contains 5 Fourier modes:

$$\begin{pmatrix} \hat{H}^{(0)} - 3\Omega & \hat{H}^{(-1)} & \hat{H}^{(-2)} & 0 & 0 & 0 & 0 & 0 \\ \hat{H}^{(1)} & \hat{H}^{(0)} - 2\Omega & \hat{H}^{(-1)} & \hat{H}^{(-2)} & 0 & 0 & 0 & 0 \\ \hat{H}^{(2)} & \hat{H}^{(1)} & \hat{H}^{(0)} - \Omega & \hat{H}^{(-1)} & \hat{H}^{(-2)} & 0 & 0 & 0 \\ 0 & \hat{H}^{(2)} & \hat{H}^{(1)} & \hat{H}^{(0)} & \hat{H}^{(-1)} & \hat{H}^{(-2)} & 0 & 0 \\ 0 & 0 & \hat{H}^{(2)} & \hat{H}^{(1)} & \hat{H}^{(0)} + \Omega & \hat{H}^{(-1)} & \hat{H}^{(-2)} & 0 \\ 0 & 0 & 0 & \hat{H}^{(2)} & \hat{H}^{(1)} & \hat{H}^{(0)} + 2\Omega & \hat{H}^{(-1)} & 0 \\ 0 & 0 & 0 & 0 & \hat{H}^{(2)} & \hat{H}^{(1)} & \hat{H}^{(0)} + 3\Omega & 0 \\ 0 & 0 & 0 & 0 & 0 & 0 & 0 & \hat{H}^{(0)} + 4\Omega \end{pmatrix}. \quad (\text{A1})$$

We see that the extended Floquet Hamiltonian  $\hat{H}_F$  has been block-diagonalized. This means that the largest-energy Floquet zone will separate out and not mix with other zones even after taking any power of  $\hat{H}_F$ .

Now, we focus on the auxiliary part of the extended Floquet Hamiltonian. We express the auxiliary matrix and auxiliary vectors in terms of the standard matrix basis. A ket vector  $|n\rangle$  in the  $n_a$ -qubit auxiliary space (of dimension  $2^{n_a} = 2(N_c + 1)$ ) can be represented in terms of the standard basis vectors as:

$$|n\rangle = e_{N_c+n+1}, \quad (\text{A2})$$

where  $-N_c \leq n \leq N_c + 1$  and  $e_{N_c+n+1} \in \{e_1, e_2, \dots, e_{2^{n_a}}\}$  is standard basis (column) vector in  $\mathbb{R}^{2^{n_a}}$  with a single non-zero entry of 1 at position  $N_c + n + 1$ . Similarly, the bra vector  $\langle n|$  corresponds to a standard basis row vector. Likewise, auxiliary matrices  $A^{(|r|)}$ , defined as

$$A^{(|r|)} = \sum_{n=-N_c}^{N_c+1-|r|} |n + |r|\rangle \langle n|, \quad (\text{A3})$$

can also be expressed in terms of the standard matrix basis in  $\mathbb{R}^{2^{n_a}} \times \mathbb{R}^{2^{n_a}}$ . Specifically, we can write:

$$|n\rangle\langle m| = E_{N_c+n+1, N_c+m+1}, \quad (\text{A4})$$

where  $n, m \in [-N_c, N_c + 1]$  and  $E_{N_c+n+1, N_c+m+1} \in \{E_{1,1}, E_{1,2}, \dots, E_{1,2^{n_a}}, \dots, E_{2^{n_a}, 2^{n_a}}\}$  is a standard matrix basis element in  $\mathbb{R}^{2^{n_a}} \times \mathbb{R}^{2^{n_a}}$ . This matrix has a single non-zero entry of 1 at the position  $(N_c + n + 1, N_c + m + 1)$ . We also have  $A^{(-|r|)} = A^{(|r|)\dagger}$ . Now, we give explicit expressions of auxiliary ket vectors as column vectors for  $n_a = 3$  qubits:

$$\begin{aligned} |-3\rangle &= (1, 0, 0, 0, 0, 0, 0, 0)^T, |-2\rangle = (0, 1, 0, 0, 0, 0, 0, 0)^T, |-1\rangle = (0, 0, 1, 0, 0, 0, 0, 0)^T, |0\rangle = (0, 0, 0, 1, 0, 0, 0, 0)^T \\ |1\rangle &= (0, 0, 0, 0, 1, 0, 0, 0)^T, |2\rangle = (0, 0, 0, 0, 0, 1, 0, 0)^T, |3\rangle = (0, 0, 0, 0, 0, 0, 1, 0)^T, |4\rangle = (0, 0, 0, 0, 0, 0, 0, 1)^T, \end{aligned} \quad (\text{A5})$$

and auxiliary bra vectors are row vectors (same as above without transpose). Now the auxiliary matrix for  $r = 1$  is:

$$A^{(1)} = \sum_{n=-3}^3 |n+1\rangle\langle n| = \begin{pmatrix} 0 & 0 & 0 & 0 & 0 & 0 & 0 & 0 \\ 1 & 0 & 0 & 0 & 0 & 0 & 0 & 0 \\ 0 & 1 & 0 & 0 & 0 & 0 & 0 & 0 \\ 0 & 0 & 1 & 0 & 0 & 0 & 0 & 0 \\ 0 & 0 & 0 & 1 & 0 & 0 & 0 & 0 \\ 0 & 0 & 0 & 0 & 1 & 0 & 0 & 0 \\ 0 & 0 & 0 & 0 & 0 & 1 & 0 & 0 \\ 0 & 0 & 0 & 0 & 0 & 0 & 1 & 0 \end{pmatrix}, \quad (\text{A6})$$

and  $A^{(-1)} = A^{(1)\dagger}$ . Similarly, the asymmetric auxiliary matrix for  $r = 1$  is:

$$A_{\text{asy}}^{(1)} = |4\rangle\langle 3| = \begin{pmatrix} 0 & 0 & 0 & 0 & 0 & 0 & 0 & 0 \\ 0 & 0 & 0 & 0 & 0 & 0 & 0 & 0 \\ 0 & 0 & 0 & 0 & 0 & 0 & 0 & 0 \\ 0 & 0 & 0 & 0 & 0 & 0 & 0 & 0 \\ 0 & 0 & 0 & 0 & 0 & 0 & 0 & 0 \\ 0 & 0 & 0 & 0 & 0 & 0 & 0 & 0 \\ 0 & 0 & 0 & 0 & 0 & 0 & 0 & 0 \\ 0 & 0 & 0 & 0 & 0 & 0 & 1 & 0 \end{pmatrix}. \quad (\text{A7})$$

## 1. Scaling of Pauli strings for off diagonal matrices in terms of auxiliary qubits

In Sec. III A of the main text, we provide the decomposition of off diagonal auxiliary matrices into Pauli strings. Here we calculate the scaling of the number of Pauli strings in these decompositions with respect to the number of auxiliary qubits  $n_a$ . For a given  $r$ , we calculate  $k_0 = \lceil \log_2(|r|) \rceil$ , and we can write the auxiliary matrix for  $n_a$  qubits as:

$$A_{n_a}^{(-|r|)} = I^{\otimes(n_a-k_0)} \otimes A_{k_0}^{(-|r|)} + \sum_{k=0}^{n_a-k_0-1} I^{\otimes k} \otimes P^+ \otimes (P^-)^{\otimes(n_a-k-k_0-1)} \otimes Q_{k_0}^{(-|r|)}, \quad (\text{A8})$$

$$A_{n_a}^{(|r|)} = I^{\otimes(n_a-k_0)} \otimes A_{k_0}^{(|r|)} + \sum_{k=0}^{n_a-k_0-1} I^{\otimes k} \otimes P^- \otimes (P^+)^{\otimes(n_a-k-k_0-1)} \otimes Q_{k_0}^{(|r|)}, \quad (\text{A9})$$

where  $A_{k_0}^{(r)}$  and  $Q_{k_0}^{(r)}$  are two unknown quantities corresponding to  $r = \pm|r|$ . We can calculate the number of Pauli strings for  $A_{k_0}^{(r)}$  and  $Q_{k_0}^{(r)}$  using Eqs. (17)–(19) of Sec. III A. After that, we can calculate the total number of Pauli strings for any auxiliary matrices under arbitrary qubit truncation. We denote the number of Pauli strings in  $A_{k_0}^{(r)}$  and  $Q_{k_0}^{(r)}$  as  $\mathcal{N}_P(A_{k_0}^{(r)})$  and  $\mathcal{N}_P(Q_{k_0}^{(r)})$  respectively. The total number of Pauli strings is:

$$\begin{aligned} \mathcal{N}_P(A_{n_a}^{(r)}) &= \mathcal{N}_P(A_{k_0}^{(r)}) + \mathcal{N}_P(Q_{k_0}^{(r)}) \sum_{n=1}^{n_a-k_0} 2^n \\ &= \mathcal{N}_P(A_{k_0}^{(r)}) + \mathcal{N}_P(Q_{k_0}^{(r)}) 2^{n_a-k_0+1} \left(1 - (1/2)^{n_a-k_0}\right). \end{aligned} \quad (\text{A10})$$

Here,  $\mathcal{N}_P(A_{k_0}^{(r)})$  and  $\mathcal{N}_P(Q_{k_0}^{(r)})$  depend on  $r$  or  $k_0$  only and not on  $n_a$ . In particular, for  $r = \pm 2^{k_0}$ , we have  $A_{k_0}^{(r)} = 0$  and  $Q_{k_0}^{(r)} = I^{\otimes k_0}$ . So,  $\mathcal{N}_P(A_{n_a}^{(r=\pm 2^{k_0})}) = 2^{n_a - k_0 + 1} (1 - (1/2)^{n_a - k_0}) \leq 2^{n_a - k_0 + 1}$ . In general, for  $n_a \gg k_0$ , we have  $\mathcal{N}_P(A_{n_a}^{(r)}) \approx O(2^{n_a})$ .

### Appendix B: Choice of initial auxiliary state

In this appendix, we prove that the choice of the initial state  $|\psi_{\text{in}}\rangle = |0\rangle \otimes |\phi_p\rangle$  as given in Eq. (23) eliminates the dependency of its squared Floquet energy on driving frequency  $\Omega$  and on the number of auxiliary qubits  $n_a$ . We begin by writing  $\hat{H}_F^2$  in terms of its dependence on  $\Omega$ :

$$\hat{H}_F^2 = I \otimes (\hat{H}^{(0)})^2 + \hat{g}_\Omega + \hat{h}, \quad (\text{B1})$$

where

$$\begin{aligned} \hat{g}_\Omega &= \Omega^2 (A^{\text{d}})^2 \otimes \hat{I} + 2\Omega (A^{\text{d}} \otimes \hat{H}^{(0)}) + \Omega \sum_{r \in \mathbb{F}} \{A^{\text{d}}, A_{\text{sym}}^{(r)}\} \otimes \hat{H}^{(r)}, \\ \hat{h} &= \sum_{r \in \mathbb{F}} A_{\text{sym}}^{(r)} \otimes \{\hat{H}^{(0)}, \hat{H}^{(r)}\} + \left( \sum_{r \in \mathbb{F}} A_{\text{sym}}^{(r)} \otimes \hat{H}^{(r)} \right)^2. \end{aligned}$$

Here,  $\{O_1, O_2\} = O_1 O_2 + O_2 O_1$  is the anti-commutator, and  $A_{\text{sym}}^{(r)} = A^{(r)} - A_{\text{asy}}^{(r)}$ . We choose  $|\psi_{\text{in}}\rangle = |0\rangle \otimes |\phi_p\rangle$ . Let us first look at the terms that depend on  $\Omega$ :

$$\begin{aligned} \langle\langle \psi_{\text{in}} | \hat{g}_\Omega | \psi_{\text{in}} \rangle\rangle &= \langle\langle \psi_{\text{in}} | \Omega^2 (A^{\text{d}})^2 \otimes \hat{I} | \psi_{\text{in}} \rangle\rangle + 2\Omega \langle\langle \psi_{\text{in}} | (A^{\text{d}} \otimes \hat{H}^{(0)}) | \psi_{\text{in}} \rangle\rangle + \langle\langle \psi_{\text{in}} | \Omega \sum_{r \in \mathbb{F}} \{A^{\text{d}}, A_{\text{sym}}^{(r)}\} \otimes \hat{H}^{(r)} | \psi_{\text{in}} \rangle\rangle \\ &= \Omega^2 \langle 0 | (A^{\text{d}})^2 | 0 \rangle \langle \phi_p | \hat{I} | \phi_p \rangle + 2\Omega \langle 0 | A^{\text{d}} | 0 \rangle \langle \phi_p | \hat{H}^{(0)} | \phi_p \rangle + \Omega \sum_{r \in \mathbb{F}} \langle 0 | \{A^{\text{d}}, A_{\text{sym}}^{(r)}\} | 0 \rangle \langle \phi_p | \hat{H}^{(r)} | \phi_p \rangle \\ &= 0. \end{aligned} \quad (\text{B2})$$

Thus this choice of the initial state removes the dependence on  $\Omega$ . Now we look at the terms of  $\hat{H}_F^2$  that do not contain  $\Omega$  but still depend on  $n_a$ :

$$\begin{aligned} \langle\langle \psi_{\text{in}} | I \otimes (\hat{H}^{(0)})^2 | \psi_{\text{in}} \rangle\rangle &= \langle 0 | I | 0 \rangle \langle \phi_p | (\hat{H}^{(0)})^2 | \phi_p \rangle \\ &= \langle \phi_p | (\hat{H}^{(0)})^2 | \phi_p \rangle. \end{aligned} \quad (\text{B3})$$

Thus, the above expectation value is independent of  $n_a$ . We also have

$$\begin{aligned} \langle\langle \psi_{\text{in}} | \hat{h} | \psi_{\text{in}} \rangle\rangle &= \langle\langle \psi_{\text{in}} | \sum_{r \in \mathbb{F}} A_{\text{sym}}^{(r)} \otimes \{\hat{H}^{(0)}, \hat{H}^{(r)}\} | \psi_{\text{in}} \rangle\rangle + \langle\langle \psi_{\text{in}} | \left( \sum_{r \in \mathbb{F}} A_{\text{sym}}^{(r)} \otimes \hat{H}^{(r)} \right)^2 | \psi_{\text{in}} \rangle\rangle \\ &= \sum_{r \in \mathbb{F}} \langle 0 | A_{\text{sym}}^{(r)} | 0 \rangle \langle \phi_p | \{\hat{H}^{(0)}, \hat{H}^{(r)}\} | \phi_p \rangle + \sum_{r, r' \in \mathbb{F}} \langle 0 | A_{\text{sym}}^{(r)} A_{\text{sym}}^{(r')} | 0 \rangle \langle \phi_p | \hat{H}^{(r)} \hat{H}^{(r')} | \phi_p \rangle \\ &= \sum_{r \in \mathbb{F}} c_1(r) \langle \phi_p | \{\hat{H}^{(0)}, \hat{H}^{(r)}\} | \phi_p \rangle + \sum_{r, r' \in \mathbb{F}} c_2(r, r') \langle \phi_p | \hat{H}^{(r)} \hat{H}^{(r')} | \phi_p \rangle, \end{aligned} \quad (\text{B4})$$

where,  $c_1(r)$  and  $c_2(r, r')$  are dependent on Fourier indices but not on  $n_a$ . Let's look at  $c_1(r)$

$$\begin{aligned} c_1(r > 0) &= \sum_{n=-N_c}^{N_c-r} \langle 0 | (|n+r\rangle \langle n|) | 0 \rangle = 0, \\ c_1(r < 0) &= \sum_{n=-N_c}^{N_c-|r|} \langle 0 | (|n\rangle \langle n+|r||) | 0 \rangle = 0. \end{aligned} \quad (\text{B5})$$

Now, we look at the  $c_2(r, r')$  corresponding to four different values of  $(r, r')$

$$\begin{aligned}
c_2(r > 0, r' > 0) &= \langle 0 | \left( \sum_{n=-N_c}^{N_c-r} |n+r\rangle \langle n| \right) \left( \sum_{m=-N_c}^{N_c-r'} |m+r'\rangle \langle m| \right) | 0 \rangle \\
&= \left( \sum_{n=-N_c}^{N_c-r} \delta_{0, n+r} \langle n| \right) \left( \sum_{m=-N_c}^{N_c-r'} |m+r'\rangle \delta_{m,0} \right) \\
&= \langle -r | r' \rangle = 0, \\
c_2(r < 0, r' < 0) &= \langle 0 | \left( \sum_{n=-N_c}^{N_c-|r|} |n\rangle \langle n+|r|| \right) \left( \sum_{m=-N_c}^{N_c-|r'|} |m\rangle \langle m+|r'|| \right) | 0 \rangle \\
&= \langle (|r|)(-|r'|) \rangle = 0, \\
c_2(r > 0, r' < 0) &= \langle 0 | \left( \sum_{n=-N_c}^{N_c-r} |n+r\rangle \langle n| \right) \left( \sum_{m=-N_c}^{N_c-|r'|} |m\rangle \langle m+|r'|| \right) | 0 \rangle \\
&= \langle -r | (-|r'|) \rangle = \delta_{r, |r'|} = \delta_{r, -r'}, \\
c_2(r < 0, r' > 0) &= \langle 0 | \left( \sum_{n=-N_c}^{N_c-|r|} |n\rangle \langle n+|r|| \right) \left( \sum_{m=-N_c}^{N_c-r'} |m+r'\rangle \langle m| \right) | 0 \rangle \\
&= \langle -r | (|r'|) \rangle = \delta_{|r|, r'} = \delta_{-r, r'}.
\end{aligned} \tag{B6}$$

Putting the above values of  $c_1(r)$  and  $c_2(r, r')$  in Eq. (B4), we obtain

$$\begin{aligned}
\langle\langle \psi_{\text{in}} | \hat{h} | \psi_{\text{in}} \rangle\rangle &= 0 + \sum_{r \in \mathbb{F}^+, r' \in \mathbb{F}^-} \langle \phi_{\text{p}} | \hat{H}^{(r)} \hat{H}^{(r')} | \phi_{\text{p}} \rangle \delta_{r, -r'} + \sum_{r' \in \mathbb{F}^+, r \in \mathbb{F}^-} \langle \phi_{\text{p}} | \hat{H}^{(r)} \hat{H}^{(r')} | \phi_{\text{p}} \rangle \delta_{-r, r'} \\
&= \sum_{r \in \mathbb{F}^+} \langle \phi_{\text{p}} | (\hat{H}^{(r)} \hat{H}^{(-r)} + \hat{H}^{(-r)} \hat{H}^{(r)}) | \phi_{\text{p}} \rangle,
\end{aligned} \tag{B7}$$

where  $\mathbb{F}^\pm$  represent the sets of positive (+) and negative (−) indices labeling the Fourier modes of the time-periodic Hamiltonian. Overall, the squared Floquet energy for the initial state is

$$\langle\langle \psi_{\text{in}} | \hat{H}_{\text{F}}^2 | \psi_{\text{in}} \rangle\rangle = \langle \phi_{\text{p}} | (\hat{H}^{(0)})^2 | \phi_{\text{p}} \rangle + \sum_{r \in \mathbb{F}^+} \langle \phi_{\text{p}} | (\hat{H}^{(r)} \hat{H}^{(-r)} + \hat{H}^{(-r)} \hat{H}^{(r)}) | \phi_{\text{p}} \rangle. \tag{B8}$$

Thus, our choice of initial state removes the dependence on both  $\Omega$  and  $n_a$  in the initial squared Floquet energy, as we claimed in Sec. III B.

Next, using numerical simulation, we look into how the squared Floquet energies of random states depend on  $\Omega$ . Figure 8 shows how the squared Floquet energy changes with the number of ADAPT iterations for four random states at  $\Omega = 35.0$  and  $n_a = 4$ . The inset shows a zoom-in over a subset of the ADAPT iterations. We find that the Floquet squared energy for random states is almost one order of magnitude larger than the results shown in Fig. 4(a) of the main text for  $\Omega = 5.0$ . Thus, we see that increasing  $\Omega$  results in a higher initial squared Floquet energy, which affects the convergence rate.



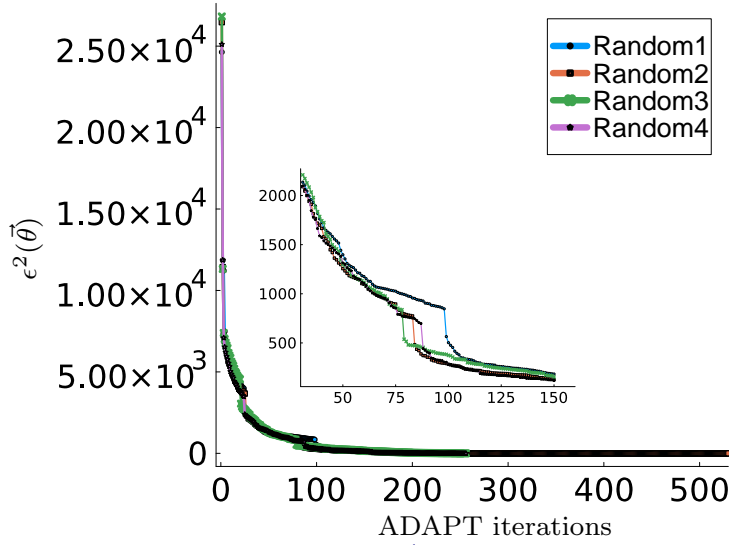


FIG. 8. Squared quasienergy  $\epsilon^2(\vec{\theta})$  versus the number of ADAPT iterations for various parameters. The inset shows a zoom-in of the first 150 iterations. All parameters are expressed in units of the characteristic coupling constant  $J_0$ . The parameters are  $L = 3, n_a = 4, \Omega = 35.0J_0, (\bar{J}_x, \bar{J}_y, \bar{J}_z) = (3.7, 2.8, 3.9)J_0, (\delta J_x, \delta J_y, \delta J_z) = (0.0, 0.0, 0.0)J_0, \bar{B}_z = 2.9J_0, \delta B_z = 2.7J_0$ . We use a mixed Floquet operator pool consisting of all possible Pauli operators on the auxiliary qubits and two-local XYZ operators on the physical qubits.

### Appendix C: Expectation value of an operator

In this appendix, we show how to calculate the expectation value of an operator in a Floquet state within the Floquet-Hilbert space. We provide detailed information regarding Eq. (24) in the main text. For a given operator  $\hat{O}$  and Floquet state  $|\psi(t)\rangle = e^{-i\epsilon t} |\phi(t)\rangle$ , we have  $\langle \hat{O}(t) \rangle_\psi = \langle \psi(t) | \hat{O} | \psi(t) \rangle = \langle \phi(t) | \hat{O} | \phi(t) \rangle = \langle \hat{O}(t) \rangle_\phi$ . We can write

$$\begin{aligned}
 \langle \hat{O}(t) \rangle_\phi &= \langle \phi(t) | \hat{O} | \phi(t) \rangle \\
 &= \left( \sum_n e^{-in\Omega t} \langle \phi^{(n)} | \right) \hat{O} \left( \sum_m e^{im\Omega t} | \phi^{(m)} \rangle \right) \\
 &= \left( \dots, \langle \phi^{(-2)} | e^{i2\Omega t}, \langle \phi^{(-1)} | e^{i\Omega t}, \langle \phi^{(0)} |, \langle \phi^{(1)} | e^{-i\Omega t}, \langle \phi^{(2)} | e^{-i2\Omega t}, \dots \right) \\
 &\quad \begin{pmatrix} \vdots \\ \hat{O} \sum_m e^{im\Omega t} | \phi^{(m)} \rangle \\ \hat{O} \sum_m e^{im\Omega t} | \phi^{(m)} \rangle \\ \hat{O} \sum_m e^{im\Omega t} | \phi^{(m)} \rangle \\ \hat{O} \sum_m e^{im\Omega t} | \phi^{(m)} \rangle \\ \hat{O} \sum_m e^{im\Omega t} | \phi^{(m)} \rangle \\ \hat{O} \sum_m e^{im\Omega t} | \phi^{(m)} \rangle \\ \vdots \end{pmatrix} \\
 &= \left( \dots, \langle \phi^{(-2)} | e^{i2\Omega t}, \langle \phi^{(-1)} | e^{i\Omega t}, \langle \phi^{(0)} |, \langle \phi^{(1)} | e^{-i\Omega t}, \langle \phi^{(2)} | e^{-i2\Omega t}, \dots \right) \\
 &\quad \begin{pmatrix} \hat{O} & \hat{O} & \hat{O} & \dots & \hat{O} & \hat{O} & \hat{O} \\ \hat{O} & \hat{O} & \hat{O} & \dots & \hat{O} & \hat{O} & \hat{O} \\ \hat{O} & \hat{O} & \hat{O} & \dots & \hat{O} & \hat{O} & \hat{O} \\ \vdots & & & & & & \vdots \\ \hat{O} & \hat{O} & \hat{O} & \dots & \hat{O} & \hat{O} & \hat{O} \\ \hat{O} & \hat{O} & \hat{O} & \dots & \hat{O} & \hat{O} & \hat{O} \\ \hat{O} & \hat{O} & \hat{O} & \dots & \hat{O} & \hat{O} & \hat{O} \end{pmatrix} \begin{pmatrix} \vdots \\ e^{-i2\Omega t} | \phi^{(-2)} \rangle \\ e^{-i\Omega t} | \phi^{(-1)} \rangle \\ | \phi^{(0)} \rangle \\ e^{i\Omega t} | \phi^{(1)} \rangle \\ e^{i2\Omega t} | \phi^{(2)} \rangle \\ \vdots \end{pmatrix}
 \end{aligned}$$

$$\begin{aligned}
&= \left( \dots, \langle \phi^{(-2)} |, \langle \phi^{(-1)} |, \langle \phi^{(0)} |, \langle \phi^{(1)} |, \langle \phi^{(2)} |, \dots \right) \hat{U}^\dagger(t) \begin{pmatrix} \hat{O} & \hat{O} & \hat{O} & \dots & \hat{O} & \hat{O} & \hat{O} \\ \hat{O} & \hat{O} & \hat{O} & \dots & \hat{O} & \hat{O} & \hat{O} \\ \hat{O} & \hat{O} & \hat{O} & \dots & \hat{O} & \hat{O} & \hat{O} \\ \vdots & & & & & & \vdots \\ \hat{O} & \hat{O} & \hat{O} & \dots & \hat{O} & \hat{O} & \hat{O} \\ \hat{O} & \hat{O} & \hat{O} & \dots & \hat{O} & \hat{O} & \hat{O} \\ \hat{O} & \hat{O} & \hat{O} & \dots & \hat{O} & \hat{O} & \hat{O} \end{pmatrix} \hat{U}(t) \begin{pmatrix} \vdots \\ |\phi^{(-2)}\rangle \\ |\phi^{(-1)}\rangle \\ |\phi^{(0)}\rangle \\ |\phi^{(1)}\rangle \\ |\phi^{(2)}\rangle \\ \vdots \end{pmatrix}. \\
&= \langle\langle \phi | \hat{U}^\dagger(t) \hat{O} \hat{U}(t) | \phi \rangle\rangle.
\end{aligned} \tag{C1}$$

Here,  $\hat{U}(t) = e^{i\Omega A^d t} \otimes \hat{I}$  applies phases to the vector elements of the extended Floquet state. We note that an element in an extended Floquet state is a vector in physical space, therefore we refer to it as a vector element. Thus, we obtain Eq. (24) in the main text. We have obtained this equation without truncating the auxiliary space. Next, we express the state and operators for the truncated case. Because our  $\hat{H}_F$  is block-diagonalized, the extended Floquet state in the central Floquet zone is:

$$|\phi\rangle = (|\phi^{(-N_c)}\rangle, \dots, |\phi^{(0)}\rangle, |\phi^{(N_c)}\rangle, \vec{0}_\phi)^T, \tag{C2}$$

where  $\vec{0}_\phi$  is  $D$ -dimensional zero vector where  $D$  is the dimension of physical Hilbert space. This implies that the truncated matrix representation of  $\hat{O}$  can have any physical operator on the last column and row without affecting the expectation values. Specifically, we choose the  $\hat{O}$  operator for the last column and row. Thus, we obtain  $\hat{O} = (I + X)^{\otimes n_a} \otimes \hat{O}$ .

#### Appendix D: Quasienergy spectra and eigenstates in a Floquet zone

In this appendix, we use an alternate method to calculate the full quasienergy spectrum within the central Floquet zone. In particular, we use a modified cost function for calculating excited states [51] that penalizes overlap with the previously found eigenstates, where the cost function for the  $k^{\text{th}}$  excited state may be written as

$$C(\vec{\theta}) = \langle\langle \Psi(\vec{\theta}) | \hat{H}_F^2 | \Psi(\vec{\theta}) \rangle\rangle + \sum_{i=0}^{k-1} \beta_i |\langle\langle \Psi(\vec{\theta}) | \Psi_i(\vec{\varphi}) \rangle\rangle|^2, \tag{D1}$$

where  $\Psi_i(\vec{\varphi})$  are the previously found eigenstates with optimized coefficients  $\vec{\varphi}$ .

This is equivalent to minimizing the objective function

$$\hat{H}_{F,k}^2 = \hat{H}_F^2 + \sum_{i=0}^{k-1} \beta_i |\Psi_i(\vec{\varphi})\rangle \langle\langle \Psi_i(\vec{\varphi})|. \tag{D2}$$

The modified cost function in Eq.(D2) leads to a modified pool operator gradient expression compared to the original expression [24]. The expression for the gradient of  $\langle\langle \hat{H}_{F,k}^2 \rangle\rangle$  with respect to pool operator  $\hat{A}_l$  is

$$\partial \langle\langle \hat{H}_{F,k}^2 \rangle\rangle / \partial \theta_l \Big|_{\theta_l=0} = i \langle\langle \Psi(\theta) | [\hat{A}_l, \hat{H}_{F,k}^2] | \Psi(\theta) \rangle\rangle + 2 \sum_{i=0}^{k-1} \beta_i (\text{Re}(x_i) \text{Im}(y_i) - \text{Im}(x_i) \text{Re}(y_i)), \tag{D3}$$

where  $x_i = \langle\langle \Psi_i(\vec{\varphi}) | \Psi(\theta) \rangle\rangle$ ,  $y_i = \langle\langle \Psi_i(\vec{\varphi}) | \hat{A}_l | \Psi(\theta) \rangle\rangle$ .

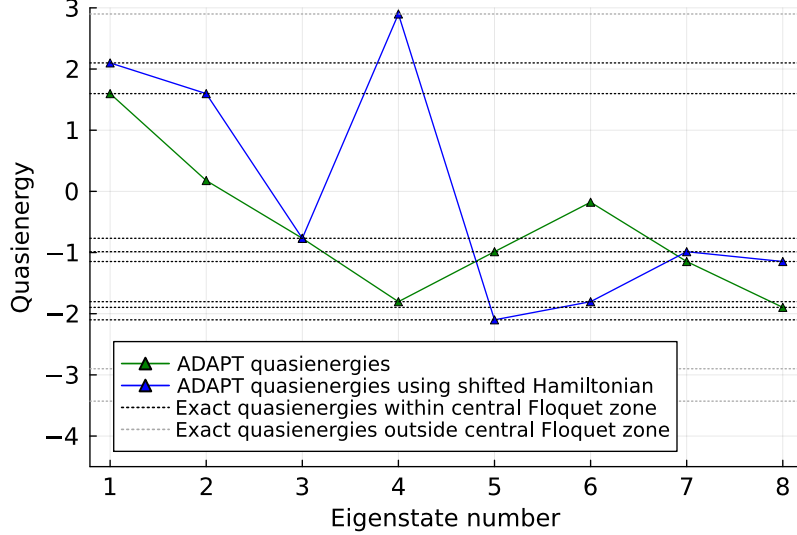


FIG. 9. Calculation of quasienergies using the Floquet-ADAPT-VQE algorithm with the modified cost function in Eq.(D2). All parameters are expressed in units of the characteristic coupling constant  $J_0$ . We consider a system with  $L = 3, n_a = 4, \Omega = 5.0J_0, (\bar{J}_x, \bar{J}_y, \bar{J}_z) = (3.7, 2.8, 3.9)J_0, (\delta J_x, \delta J_y, \delta J_z) = (1.9, 1.1, 1.2)J_0, \bar{B}_z = 2.9J_0, \delta B_z = 2.7J_0$ . The reference state used here is an equal superposition of all computational basis states,  $|+\rangle^{\otimes L_{tot}}$ . The shift parameter used to obtain the blue data is  $\lambda = 0.6J_0$ .

The results of using the cost function Eq.(D2) in Floquet-ADAPT-VQE to calculate the quasienergy spectra in the central Floquet zone for a system with  $L = 3, n_a = 4$  are shown in Fig. 9. For these simulations, we use an operator pool consisting of all possible two-local XYZ Pauli strings on the total number of qubits,  $L + n_a$ . The low support of each pool operator lends itself to the strategy of adding multiple disjoint operators at each ADAPT iteration, and these simulations are run using TETRIS-ADAPT-VQE [26]. The eigenenergies found by Floquet-ADAPT-VQE are depicted in green. Although they are not obtained in an increasing manner, the algorithm is able to find six of the eight exact quasienergies in the central Floquet zone, which are shown as black dotted horizontal lines. The other two quasienergies found by the algorithm correspond to energies of states that are degenerate in the spectrum of the cost function with the squared Floquet Hamiltonian in Eq. (D2). The degeneracy in the spectrum leads the algorithm to find a linear combination of the two states, where the linear combination may not be an eigenstate of the Floquet Hamiltonian. The problem associated with the degeneracy can be mitigated by adding a small shift to the Floquet Hamiltonian as discussed in Sec. III B,  $\hat{H}_F \rightarrow (\hat{H}_F - \lambda \hat{I})$  before squaring it in Eq. (D2). This leads to the spectrum shown in blue. Note that this is a one-time shift to the Hamiltonian that is not varied. Here, the algorithm finds seven of the eight exact quasienergies in the central Floquet zone, with one corresponding to a quasienergy outside the central Floquet zone.

### Appendix E: Some details of detection of time crystal

In this appendix, we elaborate on the possibility of detecting time crystals as briefly discussed in Sec. V. Using Floquet ADAPT-VQE, we prepare an extended Floquet state with quasienergy  $\epsilon_1 < 0$  such that  $|\psi(\vec{\theta}_1)\rangle = \hat{U}(\vec{\theta}_1)|\psi_{in}\rangle$  where  $|\psi_{in}\rangle$  is the initial state. This yields the quantum unitary operator  $\hat{U}(\vec{\theta}_1)$ . We separately prepare a state with a shift parameter  $\lambda = \epsilon_1 + \Omega/2$ . We repeat this for various sets of disorder couplings. Now we repeat whole process for as many eigenstates as we can. If we find that the lowest quasienergy is zero in this shifted framework for all considered eigenstates, then we can say that the system would most likely show time crystalline behavior. Furthermore, we can detect the spontaneous breaking of symmetry by taking the expectation values of local operators. Let  $|\psi_1\rangle, |\psi_2\rangle$  be two Floquet states (their respective extended states are  $|\psi_1\rangle, |\psi_2\rangle$ ) with a quasienergy separation of  $\Omega/2$ . The steady state in the time crystal is a superposition of these two states, given by  $|\psi\rangle = |\psi_1\rangle + |\psi_2\rangle$ . Then stroboscopic

expectation value of a local operator  $\hat{O}$  in the steady state is:

$$\begin{aligned}\langle\psi(nT)|\hat{O}|\psi(nT)\rangle &= \sum_{j=1}^2 \langle\psi_j|\hat{O}|\psi_j\rangle + \text{Re}\{e^{-in\Omega T/2} \langle\psi_1|\hat{O}|\psi_2\rangle\} \\ &= \sum_{j=1}^2 \langle\psi_j|\hat{O}|\psi_j\rangle + (-1)^n \text{Re}\{ \langle\psi_1|\hat{O}|\psi_2\rangle\}.\end{aligned}\tag{E1}$$

Here,  $\text{Re}$  denotes the real part of a complex number. We can calculate the stroboscopic expectation value of the first term of the above equation using a quantum circuit (without the single-qubit  $z$ -rotations) discussed in the main text. We can calculate the second term as discussed in [61].

- 
- [1] F. Wilczek, *Phys. Rev. Lett.* **109**, 160401 (2012).
  - [2] D. V. Else, B. Bauer, and C. Nayak, *Physical review letters* **117**, 090402 (2016).
  - [3] N. Y. Yao, A. C. Potter, I.-D. Potirniche, and A. Vishwanath, *Phys. Rev. Lett.* **118**, 030401 (2017).
  - [4] V. Khemani, A. Lazarides, R. Moessner, and S. L. Sondhi, *Phys. Rev. Lett.* **116**, 250401 (2016).
  - [5] B. Li, J. S. Van Dyke, A. Warren, S. E. Economou, and E. Barnes, *Phys. Rev. B* **101**, 115303 (2020).
  - [6] E. Barnes, J. M. Nichol, and S. E. Economou, *Phys. Rev. B* **99**, 035311 (2019).
  - [7] A. Kumar, R. Frantzeskakis, and E. Barnes, *Phys. Rev. B* **111**, 014302 (2025).
  - [8] R. Frantzeskakis, J. Van Dyke, L. Zaporski, D. A. Gangloff, C. Le Gall, M. Atatüre, S. E. Economou, and E. Barnes, *Phys. Rev. B* **108**, 075302 (2023).
  - [9] N. H. Lindner, G. Refael, and V. Galitski, *Nature Physics* **7**, 490 (2011).
  - [10] A. C. Potter, T. Morimoto, and A. Vishwanath, *Phys. Rev. X* **6**, 041001 (2016).
  - [11] T. Kitagawa, E. Berg, M. Rudner, and E. Demler, *Phys. Rev. B* **82**, 235114 (2010).
  - [12] J. K. Asbóth, B. Tarasinski, and P. Delplace, *Phys. Rev. B* **90**, 125143 (2014).
  - [13] M. Rodriguez-Vega, A. Kumar, and B. Seradjeh, *Phys. Rev. B* **100**, 085138 (2019).
  - [14] T. Oka and S. Kitamura, *Annual Review of Condensed Matter Physics* **10**, 387 (2019).
  - [15] A. Kumar, G. Ortiz, P. Richerme, and B. Seradjeh, *Phys. Rev. Lett.* **126**, 206602 (2021).
  - [16] R. P. Feynman, *International Journal of Theoretical Physics* **21**, 467 (1982).
  - [17] J. Zhang, G. Pagano, P. W. Hess, A. Kyprianidis, P. Becker, H. Kaplan, A. V. Gorshkov, Z. X. Gong, and C. Monroe, *Nature* **551**, 601 (2017).
  - [18] H. Bernien, S. Schwartz, A. Keesling, H. Levine, A. Omran, H. Pichler, S. Choi, A. S. Zibrov, M. Endres, M. Greiner, V. Vuletić, and M. D. Lukin, *Nature* **551**, 579 (2017).
  - [19] G. Semeghini, H. Levine, A. Keesling, S. Ebadi, T. T. Wang, D. Bluvstein, R. Verresen, H. Pichler, M. Kalinowski, R. Samajdar, A. Omran, S. Sachdev, A. Vishwanath, M. Greiner, V. Vuletić, and M. D. Lukin, *Science* **374**, 1242 (2021).
  - [20] D. S. Abrams and S. Lloyd, *Phys. Rev. Lett.* **83**, 5162 (1999).
  - [21] J. Preskill, *Quantum* **2**, 79 (2018).
  - [22] A. Peruzzo, J. McClean, P. Shadbolt, M.-H. Yung, X.-Q. Zhou, P. J. Love, A. Aspuru-Guzik, and J. L. O'Brien, *Nature Communications* **5**, 4213 (2014).
  - [23] J. R. McClean, J. Romero, R. Babbush, and A. Aspuru-Guzik, *New Journal of Physics* **18**, 023023 (2016).
  - [24] H. R. Grimsley, S. E. Economou, E. Barnes, and N. J. Mayhall, *Nature Communications* **10**, 3007 (2019).
  - [25] H. L. Tang, V. Shkolnikov, G. S. Barron, H. R. Grimsley, N. J. Mayhall, E. Barnes, and S. E. Economou, *PRX Quantum* **2**, 020310 (2021).
  - [26] P. G. Anastasiou, Y. Chen, N. J. Mayhall, E. Barnes, and S. E. Economou, *Phys. Rev. Res.* **6**, 013254 (2024).
  - [27] H. R. Grimsley, G. S. Barron, E. Barnes, S. E. Economou, and N. J. Mayhall, *npj Quantum Information* **9**, 19 (2023).
  - [28] B. Fauseweh and J.-X. Zhu, *Quantum* **7**, 1063 (2023).
  - [29] D. Wecker, M. B. Hastings, and M. Troyer, *Phys. Rev. A* **92**, 042303 (2015).
  - [30] R. B. Griffiths and C.-S. Niu, *Phys. Rev. Lett.* **76**, 3228 (1996).
  - [31] G. Floquet, *Annales scientifiques de l'É.N.S., 2e série* **12**, 47 (1883).
  - [32] J. H. Shirley, *Physical Review* **138**, B979 (1965).
  - [33] H. Sambe, *Phys. Rev. A* **7**, 2203 (1973).
  - [34] M. Rodriguez-Vega, M. Lentz, and B. Seradjeh, *New Journal of Physics* **20**, 093022 (2018).
  - [35] A. Smith, M. S. Kim, F. Pollmann, and J. Knolle, *npj Quantum Information* **5**, 106 (2019).
  - [36] M. Ramôa, P. G. Anastasiou, L. P. Santos, N. J. Mayhall, E. Barnes, and S. E. Economou, *npj Quantum Information* **11**, 86 (2025).
  - [37] R. C. Farrell, M. Illa, A. N. Ciavarella, and M. J. Savage, *PRX Quantum* **5**, 020315 (2024).
  - [38] E. Gustafson, K. Sherbert, A. Florio, K. Shirali, Y. Chen, H. Lamm, S. Valgushev, A. Weichselbaum, S. E. Economou, R. D. Pisarski, and N. M. Tubman, *Surrogate constructed scalable circuits adapt-vqe in the schwinger model* (2024), [arXiv:2408.12641](https://arxiv.org/abs/2408.12641) [quant-ph].

- [39] G. Gyawali and M. J. Lawler, [Phys. Rev. A \*\*105\*\*, 012413 \(2022\)](#).
- [40] J. S. Van Dyke, K. Shirali, G. S. Barron, N. J. Mayhall, E. Barnes, and S. E. Economou, [Phys. Rev. Res. \*\*6\*\*, L012030 \(2024\)](#).
- [41] A. Warren, L. Zhu, N. J. Mayhall, E. Barnes, and S. E. Economou, [Adaptive variational algorithms for quantum gibbs state preparation](#) (2022), [arXiv:2203.12757 \[quant-ph\]](#).
- [42] Y. S. Yordanov, C. H. W. Barnes, and D. R. M. Arvidsson-Shukur, [Phys. Rev. A \*\*106\*\*, 032434 \(2022\)](#).
- [43] N. Gomes, A. Mukherjee, F. Zhang, T. Iadecola, C.-Z. Wang, K.-M. Ho, P. P. Orth, and Y.-X. Yao, [Advanced Quantum Technologies \*\*4\*\*, 2100114](#).
- [44] Y.-X. Yao, N. Gomes, F. Zhang, C.-Z. Wang, K.-M. Ho, T. Iadecola, and P. P. Orth, [PRX Quantum \*\*2\*\*, 030307 \(2021\)](#).
- [45] B. M. T.O. Levante, M. Baldus and R. Ernst, [Molecular Physics \*\*86\*\*, 1195 \(1995\)](#).
- [46] K. Mizuta and K. Fujii, [Quantum \*\*7\*\*, 962 \(2023\)](#).
- [47] M. S. Rudner and N. H. Lindner, [The floquet engineer's handbook](#) (2020), [arXiv:2003.08252 \[cond-mat.mes-hall\]](#).
- [48] In Section IIB of Ref. [47], the many-body energy bandwidth,  $\mathcal{W}$ , can be expressed as  $LJ_{\max}$ , where  $J_{\max}$  represents the maximum value of a local energy parameter, such as coupling terms or driving terms. By ensuring that  $LJ_{\max} \ll N_c\Omega$ , one can achieve arbitrary accuracy. Consequently, for our cases, we can use  $n_a = C \log_2(LJ_{\max}/\Omega)$ , where  $C$  is a constant that is inversely proportional to the desired accuracy.
- [49] K. Mizuta, [Phys. Rev. Res. \*\*7\*\*, 013068 \(2025\)](#).
- [50] L. Wang and A. Zunger, [The Journal of Chemical Physics \*\*100\*\*, 2394 \(1994\)](#).
- [51] O. Higgott, D. Wang, and S. Brierley, [Quantum \*\*3\*\*, 156 \(2019\)](#).
- [52] Y. S. Yordanov, V. Armaos, C. H. W. Barnes, and D. R. M. Arvidsson-Shukur, [Communications Physics \*\*4\*\*, 228 \(2021\)](#).
- [53] V. O. Shkolnikov, N. J. Mayhall, S. E. Economou, and E. Barnes, [Quantum \*\*7\*\*, 1040 \(2023\)](#).
- [54] P. Gokhale, O. Angiuli, Y. Ding, K. Gui, T. Tomesh, M. Suchara, M. Martonosi, and F. T. Chong, [Minimizing state preparations in variational quantum eigensolver by partitioning into commuting families](#) (2019), [arXiv:1907.13623 \[quant-ph\]](#).
- [55] V. Verteletskyi, T.-C. Yen, and A. F. Izmaylov, [The Journal of Chemical Physics \*\*152\*\*, 124114 \(2020\)](#).
- [56] O. Crawford, B. v. Straaten, D. Wang, T. Parks, E. Campbell, and S. Brierley, [Quantum \*\*5\*\*, 385 \(2021\)](#).
- [57] T.-C. Yen and A. F. Izmaylov, [PRX Quantum \*\*2\*\*, 040320 \(2021\)](#).
- [58] M. Rodriguez-Vega, E. Carlander, A. Bahri, Z.-X. Lin, N. A. Sinitsyn, and G. A. Fiete, [Phys. Rev. Res. \*\*4\*\*, 013196 \(2022\)](#).
- [59] A. Kumar, M. Rodriguez-Vega, T. Pereg-Barnea, and B. Seradjeh, [Phys. Rev. B \*\*101\*\*, 174314 \(2020\)](#).
- [60] A. Kumar, Y. Li, and B. Seradjeh, [arXiv e-prints](#), [arXiv:2207.02830 \(2022\)](#), [arXiv:2207.02830](#).
- [61] Z.-H. Huang, P. He, L.-J. Lang, and S.-L. Zhu, [Phys. Rev. A \*\*107\*\*, 052205 \(2023\)](#).